Living on the Edge: How traits of ecosystem engineers drive bio-physical interactions at coastal wetland edges

Gillis LG[1], Maza M[2], Garcia-Maribona J[2], Lara JL[2], Suzuki T[3], Argemi Cierco M[4], Paul M[5], Folkard AM[6], Balke T[4].

AFFILIATIONS

[1]IMDC, Van Immerseelstraat 66, 2018 Antwerpen, Belgium
[2] IH Cantabria Parque Científico y Tecnológico de Cantabria, C. Isabel Torres, 15, 39011 Santander, Cantabria, Spain
[3]Flanders Hydraulics Research, 2140 Antwerp, Belgium
[4]School of Geographical and Earth Sciences, University of Glasgow, G128QQ, Glasgow, United Kingdom
[5]Leibniz University Hannover, Ludwig-Franzius-Institute for Hydraulic, Estuarine and Coastal Engineering, Nienburger Str. 4, Hannover, Germany
[6]Lancaster Environment Centre, Lancaster University, Lancaster LA1 4YQ, United Kingdom

Highlights

- Rigid vegetation patches effectively buffer hydrodynamic energy and increase erosion at their edges.
- Flexible vegetation patches accumulate sediment closer to their leading edges compared to rigid vegetation for all hydrodynamic conditions tested.
- Negative feedbacks may compromise the lateral extension of both types of vegetation.
- Lower shoot density causes sediment accumulation to occur further inside vegetation patches.

Abstract

Salt marshes and mangrove forests provide critical ecosystem services such as reduced sediment erosion and increased hydrodynamic buffering. Sediment transport and hydrodynamics can be influenced by specific functional traits of the plants (for example, flexibility vs. rigidity) and community traits (for example, spatial density). While there is a growing body of literature on plant trait and hydrodynamic interactions, direct comparative studies of sediment transport and scour development in and around intertidal wetland edges are scarce. In this study we systematically compared the effects of plant traits on sediment budgets around the lateral edges of intertidal wetlands under controlled hydrodynamic and sedimentary conditions using full scale vegetation mimics with contrasting flexibilities and densities. Experiments were carried out in a large-scale flume, using two spatial densities each of flexible and rigid vegetation mimics. We measured unconsolidated sedimentary bed-level changes in experimental runs using waves only, currents only, and waves combined with currents. Both mimic types dampened the energy of the incoming flow, highlighting the role of rigid and flexible aquatic vegetation in providing coastal protection. The rigid vegetation mimics' lateral edge experienced larger velocities, more energetic turbulence, and local scour around individual stems. Scour around stems could influence the lateral expansion of the rigid vegetation ecosystem by reducing sediment stability and thus decreasing seedling establishment success. The flexible plant mimics produced lower turbulence at their leading edge, which resulted in sediment being deposited over a shorter distance into the patch than in the rigid mimics. Decreased vegetation density caused reduced sediment erosion at the leading edge and less sediment accumulation within the vegetation patches for both the rigid and flexible mimics. The hydrodynamic and sedimentary processes identified for both ecosystems are linked to different feedbacks. A positive feedback was identified in which vegetation attenuates hydrodynamic energy allowing sediment accumulation within the patch. A negative feedback was identified where large velocities caused flow divergence and erosion outside of the vegetation, and would therefore compromise its lateral expansion. High densities of rigid vegetation enhance this negative feedback. Lower density flexible vegetation, however, combined with less energetic hydrodynamic conditions facilitate the expansion of vegetation patches as they cause less flow divergence and therefore less

erosion. The strong flow divergence observed in the rigid vegetation cases highlight their importance for buffering hydrodynamics but at the cost of increased erosion within the front end of patches and along their lateral edges.

Keywords

Waves, currents, sediment transport, mangrove forest, salt marsh, positive and negative feedbacks, scale-dependant feedbacks

1. Introduction

Coastal intertidal wetlands are highly productive ecosystems that provide multiple ecosystem services such as coastal protection and erosion control (Barbier, 2007; Himes-Cornell et al., 2018; Mitsch and Gosselink, 2015). Ecosystem engineering species (i.e., species that physically modify the abiotic environment, *sensu* Jones et al., 1994) growing in coastal wetlands, such as mangrove trees and salt marsh grasses, form the final (semi-) terrestrial frontier facing the sea (Figure 1).

Figure 1 View of a lateral channel in a salt marsh (left panel) and a mangrove forest (right panel). Blue arrows display flow direction.

Plant and community traits of the dominant plant species in such ecosystems drive processes such as wave attenuation, current speed reduction and sediment trapping, (Moeller et al. 2014; Quartel et al. 2007; Temmerman et al. 2013). Wetlands' ability to adapt to sea-level rise through aggradation (vertical growth) and progradation (horizontal, seaward growth) (Balke et al., 2014; Wang and Temmerman, 2013; Xi) has led to increased interest in their use against coastal flooding, erosion control and as a carbon sink (Barbier, 2007; Cheong et al., 2013; Narayan et al., 2016; Vuik et al., 2016).

Hydrodynamic buffering and sediment transport is controlled by plant and community traits of the key ecosystem engineering species (Fromard et al., 1998; Jones et al., 1994; Pinsky et al., 2013; Quang Bao, 2011; Shepard et al., 2011). Plant traits (e.g., flexibility or rigidity) and community traits (e.g., stem or root spatial density) alter wave energy attenuation, flow diversion and turbulence, which in turn modifies sediment transport, deposition, and erosion. Although salt marshes and mangrove forests occupy the same physical environment (the intertidal zone), the density and flexibility of their vegetation fundamentally differ. For example, flexible vegetation could change its frontal area with the intensity of the flow and sway with wave orbital velocities causing scale dependant feedbacks such as hydrodynamic energy attenuation which enhances sediment accretion through or the formation of troughs restricting lateral expansion (Bouma et al., 2007). In contrast, rigid vegetation does not deform significantly, even in fast currents. Therefore, hydrodynamic forcing (waves and currents) and the plant and community traits (especially flexibility and density) can have implications for the geomorphological development of coastal wetlands.

Sediment dynamics around aquatic vegetation can impact the lateral development of these ecosystems. The position of a wetland's seaward edge is determined by the ecosystem's tolerance to tidal inundation and hydrodynamic forcing. Flow reduction causes sediment accumulation in intertidal wetlands can provide their plants with nutrients at the plant scale and be a carbon sink mechanism at the ecosystem scale. However, high rates of sediment accumulation may bury the plants or increase the elevation of the ecosystem so that it is outside the range suitable for optimum growth (Bouma et al., 2005). Sediment trapping within a patch can be facilitated by plant density, plant flexibility and patch size (Bouma et al., 2009). However, Bouma et al. (2009) found that there is a density threshold below which erosion around individual stems occurs. High sediment erosion can destabilise plants and constrain lateral ecosystem expansion (Widdows et al., 2008). The distribution of plant biomass amongst individual plants plays an important role in this respect. Bouma at al. 2007 in a field experiment found that rigid bamboo sticks had higher erosion within their patches compared to flexible *Spartina anglica* which displayed a dome shaped elevation pattern. Wider and deeper scour holes have also been observed around rigid cylinders in comparison to flexible plants, which by bending reduce the projected area of the plant and thus cause less scour (Yagci et al., 2016). Mangrove trees and salt marsh plants occupy different volumes of the water column due to their varying physical structures; this difference will impact on their interactions with hydrodynamics and sediment dynamics.

Despite the importance of wetlands, little is known about the feedbacks between ecosystem traits, hydrodynamic buffering or sediment transport (Hu et al., 2014; Morris et al., 2002). Feedbacks between ecosystem traits and their physical environment the expansion of the ecosystem, channel configuration and ecosystem stability (Fagherazzi et al., 2017; Liu et al., 2020; Temmink et al., 2020). Hydrodynamic effects on wetlands varies with the traits of the ecosystem engineers for instance rigid vegetation which extends through the entire water column will more strongly deflect flow velocity compared to flexible vegetation. This stronger deflection can cause a negative feedback such as larger channel erosion, which restricts lateral growth (Bouma et al., 2009). Flexible wetland plant's ability to reduce wave energy and flow velocity combined with their flexible leaves (which trap suspended particulate material) can form a positive feedback which increases sediment accumulation potential therefore nutrient availability or ecosystem expansion (Bouma et al., 2009). Another critical feedback is scale dependant feedbacks which combines both positive and negative feedbacks and is driven by wave and currents, community, and plant traits of the vegetation (Bouma et al. 2013). The combination of negative (increased erosion) and positive feedbacks (sediment accumulation) are important for organisation and distribution of salt marsh and mangrove patches. Understanding processes at the lateral edge of intertidal wetlands offers improved predictability of edge dynamics and hence the potential future seaward extent of mangrove forests and salt marshes under changing hydrodynamic forcing.

Here, we provide a direct comparative study of sediment transport and scour development at the lateral edge of such contrasting habitat types. Systematic comparisons of flexible vegetation (i.e., marsh plants) with rigid vegetation (i.e., mangrove trees) can offer new insights into sediment transport, coastal management, and the evolution of coastal wetland habitats. This study aims to contribute to knowledge by systematically comparing the effects of different plant traits on sediment dynamics, under controlled hydrodynamic and sedimentary conditions, using full scale vegetation mimics of simplified geometry to control plant flexibility and density in a large-scale laboratory flume setting. A particular focus is placed on scour development and turbulence generation near the ocean-facing and lateral edges of continuous patches bordering channels within the vegetation stand (Fig. 1). The study includes waves-only, currents-only, and combined wave-current scenarios, to explore the context dependency of bio-physical interactions in the intertidal zone. The plants' traits will influence the intensity and scale of their turbulent interactions with their physical environment. To further understand the ability of wetland ecosystems to buffer hydrodynamics and their lateral expansion, information is required on wetland feedback processes. This knowledge will allow us to predict the response of coastal wetlands to changing hydrodynamics and therefore use them further in more climate resilient coastal defences.

2. Material and Methods

The experiments were conducted in a customized wave basin at the Danish Hydraulic Institute (DHI) in Hørsholm, Denmark. The basin was 25 m wide and 35 m long, had a 5.5 m wide piston-type paddle for wave generation, and a recirculation system for current generation. Based on the facility's capabilities, along with the desired hydrodynamic conditions of an effective water depth (h) of 0.30 m and a unidirectional flow speed (U) of 0.30 ms^{-1}, the test zone was limited to a width of 5.5 m by two side walls. The area was divided into two 2.75 m wide channels with one of the ecosystem mimics placed in each one. Each of these channels was divided longitudinally into a section 1.25 m wide, in which vegetation mimics were placed, and an unvegetated section 1.50 m wide (Figure 2). This setup mimics the geometry of a channel in the vegetation stand. Given the confinement of the flume, only half a channel side was mimicked while the other side was bordered by a vertical wall. This setup allowed clear identification of the effects of the lateral and longitudinal edge of one mimic patch while free flow was able to develop in the open channel as would be the case in the centre of natural channels. At the end of the test zone, a dissipation beach was installed, consisting of several perforated, parabolic steel plates.

For the analysis of the results, a coordinate system was adopted in which X denotes the along-channel direction, with X = 0 at the upstream edge of the vegetation patches, and Y denotes the across-channel direction, with Y = 0 at the wall next to the flexible mimic section. The boundaries between the vegetated and unvegetated sections aligned in the X-direction are referred to as lateral edges (Figure 2 purple lines). The edges of the vegetation sections aligned in the Y-direction and located at X = 0 are referred to as leading edges (Figure 2 yellow lines). A schematic representation of the experimental set-up is given in Figure 2.

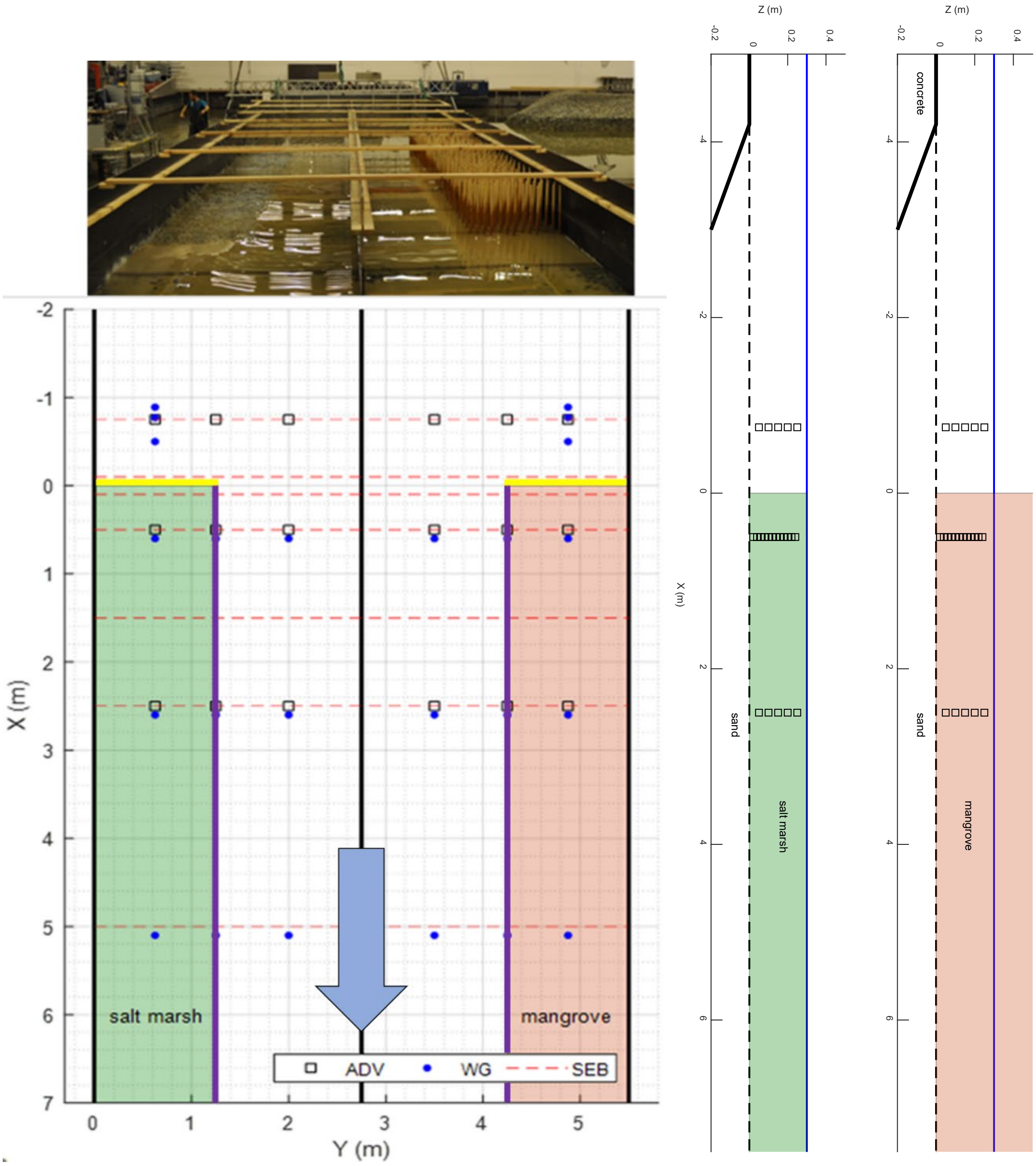

Figure 2. View of the channel from downstream (top) and schematic description of the experimental set-up (bottom). In the bottom panel, the positions of the Acoustic Doppler Velocimeters (empty squares), Wave Gauges (blue dots) and Sedimentation-Erosion Bars (red-dashed lines) are represented. The flexible and rigid vegetated areas are displayed as green and brown shaded areas. Yellow lines are the leading edges and purple lines are the lateral edges. The entire set-up (i.e., mimic vegetation patches, channels) were located within a 20 cm pit filled with sediment. The large blue arrow indicates flow direction.

2.1 Hydrodynamic conditions and sediment characteristics

Within the constraints of the facility's capabilities, the hydrodynamic conditions were defined to represent realistic inter-tidal flow conditions under mild conditions (Brinkman, 2007; Garzon et al., 2019). A water depth of 0.30 m was set, and regular waves with height H = 0.08 m and periods (T) ranging from 0.8 to 1.4 s were studied. For the experimental runs using unidirectional currents, the mean flow speed was set at 0.30 ms^{-1}. Table 1 presents the hydrodynamic conditions assigned for each run.

Table 1. Hydrodynamic conditions tested during the experiment. For the Run ID's, CC denotes currents only, WW denotes waves only and WC denotes waves combined with currents.

Run ID	***Current*** *(ms^{-1})*	***Wave Height*** *(m)*	***Wave period*** *(s)*
CC	0.30	-	-
WW1	-	0.08	0.8
WW2	-	0.08	1.1
WW3	-	0.08	1.4
WC1	0.30	0.08	0.8
WC2	0.30	0.08	1.1
WC3	0.30	0.08	1.4

The sediment was selected based on these hydrodynamic conditions. A 0.18 mm nominal diameter sand was chosen for the experiment to achieve moderate sediment transport under the test conditions. The maximum scour around the mimics was estimated based on Headie and Herbich (1986) and to prevent the scour from reaching the concrete bottom of the basin, the whole setup was placed in a 20 cm pit that was filled with sediment (Figure 2).

2.2 Vegetation mimics

Given the chosen hydrodynamic conditions, it was estimated that a 10 m length of vegetation mimic patch would be sufficient for a fully developed flow to develop within it, based on Zhang et al. (2015) and Maza et al. (2017). To exclude effects caused by traits other than the ones under investigation (flexibility and density), a simple plant mimic geometry was chosen. It consisted of circular cylinders, either rigid or flexible, with uniform vertical cross-sections. While the mimics do not resemble any specific plant species, individual (i.e., diameter, length) as well as community (i.e., density) traits were chosen similar to salt marsh vegetation for the flexible mimics and mangrove aerial roots for the rigid mimics, respectively (Table 2). The flexible mimics were defined based on the properties of salt marsh vegetation (e.g., *Salicornia* sp.) reported in the literature. To simulate basic salt marsh morphology, transparent PVC tubes of 6 mm in diameter and 50 cm in length with a Young's modulus equal to 2.9 GPa were selected based on reports such as Zhu et al. (2020). Two densities equal to 420 and 210 stems m^2 are selected for the experiments which fall within the range of natural observations (e.g., Knutson et al., 1982). Rigid mimics were defined based on mangrove prop roots properties. Mangrove roots were idealized using uniform cylinders of 3 cm diameter and long enough to be emergent under all tested conditions, based on data reported in the literature (e.g., Ohira et al., 2013). As a point of comparison, it is considered that the frontal area in both species will remain constant. Then, a density equal to 84 and 42 mimics m^2 is considered in the rigid canopy (Table 2). Shoot densities were halved for additional test runs to cover densities relevant for stages of patch development. This resulted in a higher total submerged volume for the rigid vegetation patch compared to the flexible vegetation patch, because of the former's greater volume to frontal area ratio. For current and wave only runs, only the higher vegetation densities were tested, for the combined wave and current runs, both the higher and lower vegetation densities were tested.

Table 2. Traits of the two types of vegetation mimics used.

	Flexible Vegetation	***Rigid Vegetation***
Diameter (m)	0.006	0.03
Length (m)	0.30	1.00
Density Low / High (stems m^{-2})	210/420	42/84
Frontal area Low / High (m^2)	0.378/0.756	0.378/0.756
Total submerged volume Low / High (m^3)	$1.78\ 10^{-3}/3.56\ 10^{-3}$	$8.91\ 10^{-3}/1.78\ 10^{-2}$
Submerged Solid Volume Fraction (ϕ) Low / High	0.006/0.012	0.030/0.060
Stem properties	Flexible	Rigid
Position in water depth	Stem height equal to the water depth	Emergent

2.3 Measurements and post-processing

Hydrodynamic measurements were begun 15 minutes after the flow and/or waves were turned on, to avoid transient start-up effects. Velocities were recorded with 6 Acoustic Doppler Velocimeters (ADVs) and free surface height with 24 resistive free surface gauges. All the sensors were synchronized and measured at 25 Hz for 90 seconds at each location. The incident hydrodynamic conditions were measured 0.75 m in front of the patch's leading edges. Velocity data were also obtained inside the vegetated sections at 0.5 m and 2.5m downstream of the patches’ edges. The free surface height was measured at approximately the same positions, as well as at 5 m downstream of the leading edge within the vegetation. At each of these along-channel positions, measurements were taken at three across-channel locations: in the centre of the vegetation patches, at their lateral edges and in the unvegetated channel (Figure 2). In the vertical direction, velocities were measured every 2 cm for the closest position to the edge and every 5 cm for the other two longitudinal positions, starting at 2 and 5 cm from the initial bed level respectively.

The measured velocity components were processed by applying four filtering strategies. Firstly, a filter based on signal quality was applied in which measurements with correlation values less than 50% were discarded. Secondly, a cut-off filter was applied to remove spikes in the velocity record over a predetermined threshold (0.55 ms^{-1} for waves, 0.7 ms^{-1} for currents and 1.2 ms^{-1} for waves and currents). These threshold values were determined by observing the time-series. Thirdly, an acceleration filter was used to suppress oscillations with accelerations larger than gravitational acceleration. Finally, a standard deviation filter was applied, removing velocity values which were more than three standard deviations from the mean velocity. The filtered values were left empty and not considered in further calculations. The mean velocity values were obtained by performing time-averaging for the current-only runs and phase-averaging for the waves-only and waves and current runs. The time-averages were applied over the whole of each recording. The phase-averages were calculated by dividing the time-series in intervals of the length of the wave period and then performing an ensemble averaging over them. 70 wave periods were used to obtain each of the phase-averages. Values of the turbulent kinetic energy (TKE) were obtained from the variation of the velocity signal around the mean or phase-averaged velocity for the current-only cases and the cases with waves, respectively. For wave only runs (WW), wave height evolution through the two high density patches was analysed by measuring the wave heights

(H) along their centerlines (Y = 0.625 m) and normalising them by the incident value (HI), obtained from the wave gauge located offshore of the patch, to give a relative wave height (H/HI). The submerged solid volume fraction, ϕ (Tanino and Nepf, 2008), was calculated as

$$\phi = \frac{Submerged\ Vegetation\ Volume}{Water\ Volume} \qquad (1)$$

The length-scale of vortex penetration, L_V (Zong and Nepf, 2011), was calculated as being inversely proportional to the frontal area per volume of the patch,

$$L_v = 0.5(C_D a)^{-1} \qquad (2)$$

where a is equal to d*N, d being the stem diameter and N the number of stems per unit area. The scale-dependent feedback (Bouma et al., 2013) was derived from the mean velocities. It is representative of the flow due to the presence of the vegetation patches and can be obtained as the difference between the mean velocities in the channel ($U_{channel}$) and inside the vegetation patches (U_{veg}), divided by the incident velocity (U_i):

$$Scale\ Dependent\ Feedback = \frac{U_{channel}}{U_i} - \frac{U_{veg}}{U_i} \qquad (3)$$

To measure bed elevation changes after each test, 60 measurements were taken across a transect at each of 10 longitudinal positions along the experimental area (shown in Figure 2). The measurements were conducted using two Sedimentation Erosion Bars (SEB) with 30 measurement points on each of them. At each point along the bar, a vertical pin was positioned that could be dropped onto the sediment surface, allowing its height (and thus the height of the sediment at that location) to be measured against the fixed height of the horizontal SEB. The distance between the measurement points was 5 cm. These measurements were made after each of the test runs, which lasted for approximately 1.5 hours, when the sediment bed had acquired a stable configuration. After each experiment, the sediment was re-levelled by moving it from the accumulation to the erosion zones to restore the initial flat configuration. To acquire a better representation of the bed level, the data were smoothed using a centred, 3-point moving average in the transversal direction.

3. Results

3.1 Uni-directional Flow

Current velocity patterns and sediment elevation were analysed for both types of high density simulated vegetation (Table 2). The flexible vegetation slows the incoming flow, reducing its speed by almost 50% by X = 2.5 m inside the patch (Figure 3 (a), top panel). The decrease in flow speed leads to sediment deposition within the patch, starting at around X = 1.0 m. Simultaneously, in the lateral channel the along-channel speed increases by more than 30% at X = 2.5 m with respect to the incoming value (Figure 3 (a), bottom panel), leading to sediment erosion. Figure 3 (b) shows that the largest lateral (Y-component) speeds are measured at the patch lateral edge at X = 0.5 m. These lateral speeds decrease further into the patch at X = 2.5 m. This decrease is the result of the flow divergence region at the leading edge of the patch, where the flow in line with the patch decelerates and a large part of the flow is diverted towards the open channel. The flow divergence produces sediment erosion at the leading edge where velocities are not yet significantly attenuated (top and central panel in Figure 3 (a)). The divergence flow extends over a distance L_D, defined as the length necessary for the velocities to be less than the incident values. From the velocity measurements, the L_D should be between X = 0.5 and 2.5 m. Taking the position of maximum sediment deposition within the patch as the location where velocities have been significantly attenuated to allow sediment accumulation, $L_D \approx 1.5$ m is estimated for the flexible vegetation, which falls well within the range implied by the velocity measurements.

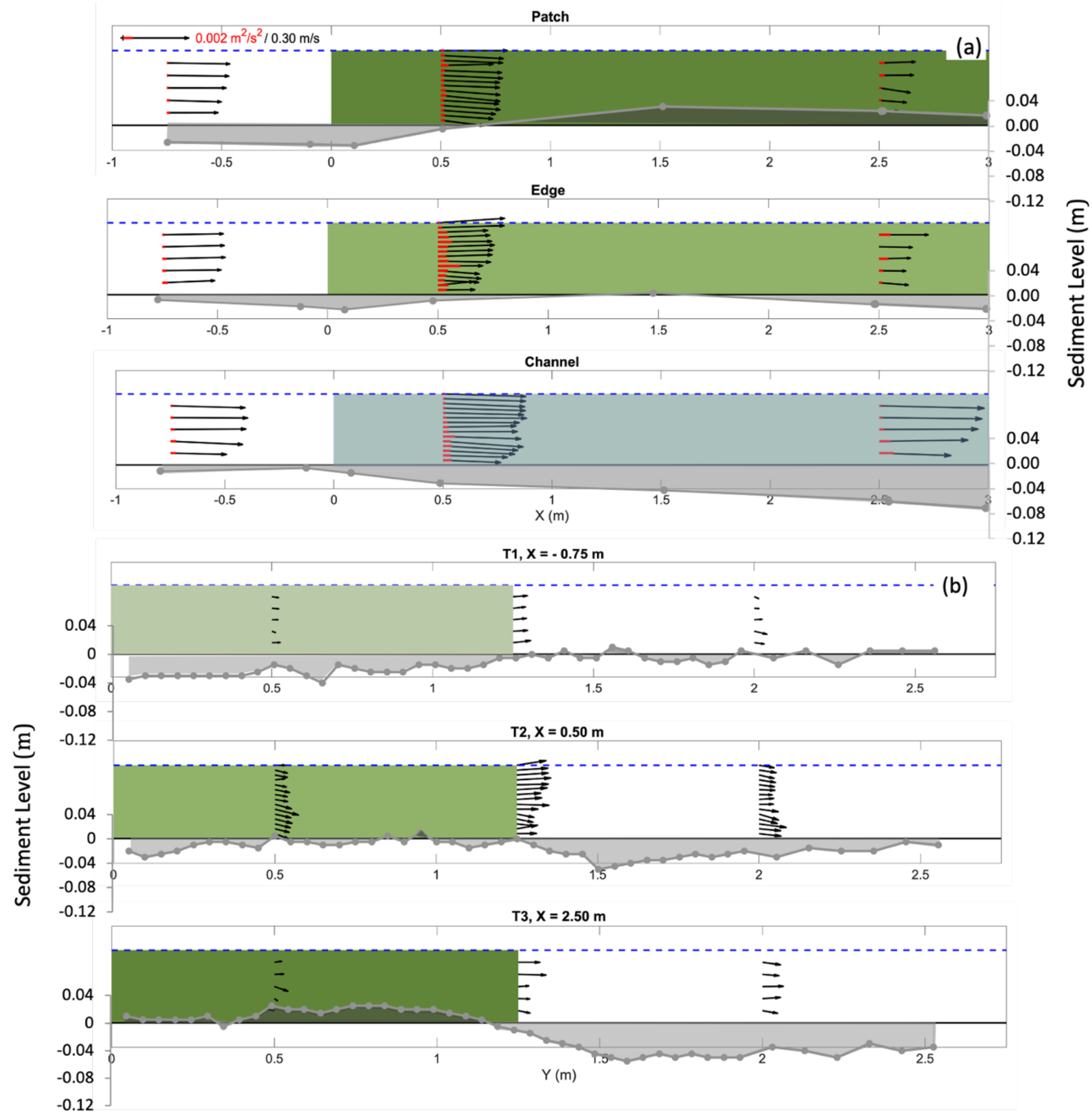

Figure 3. Flow velocity (black arrows), TKE magnitude (red lines) and sediment elevation (grey lines) for flexible vegetation and CC (currents only): a) longitudinal sections (inside the patch Y = 0.625 m, dark green, at the lateral edge Y = 1.25 m, light green, and at the channel Y = 2.00 m, blue) and (b) cross sections (at T1 X = -0.75 m, T2 X = 0.50 m, and T3 X = 2.50 m). (a) displays velocity profiles obtained using X and Z components and (b) profiles considering Y and Z components. Sediment erosion elevation is represented by light grey shading, whilst accumulation is dark grey shading. Water level (0.3 m) is presented by a dashed blue line.

In the rigid vegetation patch, Figure 4 (a) shows that the along-channel speed decreases by almost 70% by X = 2.5 m, while it increases by almost 60% within the open channel at the same X position, compared to the incoming value. Thus, the rigid vegetation produces stronger flow divergence than that observed in the flexible vegetation. Maximum lateral speeds are observed at the patch lateral edge at X = 0.5 m (Figure 4 (b)). These strong lateral speeds implies that rigid vegetation causes a major deviation of the flow around the vegetation patch. This process is also observed when analysing the free surface gradient, $\partial h/\partial x$, (produced by both patches (Figure S1). $\partial h/\partial x$ for rigid vegetation is 0.0063 (±0.0008), while for flexible vegetation it is 0.0046 (±0.0001). The largest free surface gradient obtained for rigid vegetation indicates a larger drag force exerted by the rigid elements on the flow in comparison to the flexible ones, which reconfigure under the flow action, as shown in Figure S2. Consequently, a larger drag length-scale is found for the rigid canopy, which also presents a greater submerged volume fraction ($\phi_R = 0.060$) in comparison to the flexible canopy ($\phi_F = 0.008$) leading to a larger flow energy attenuation (Mazda et al. 1997; Maza et al. 2019).

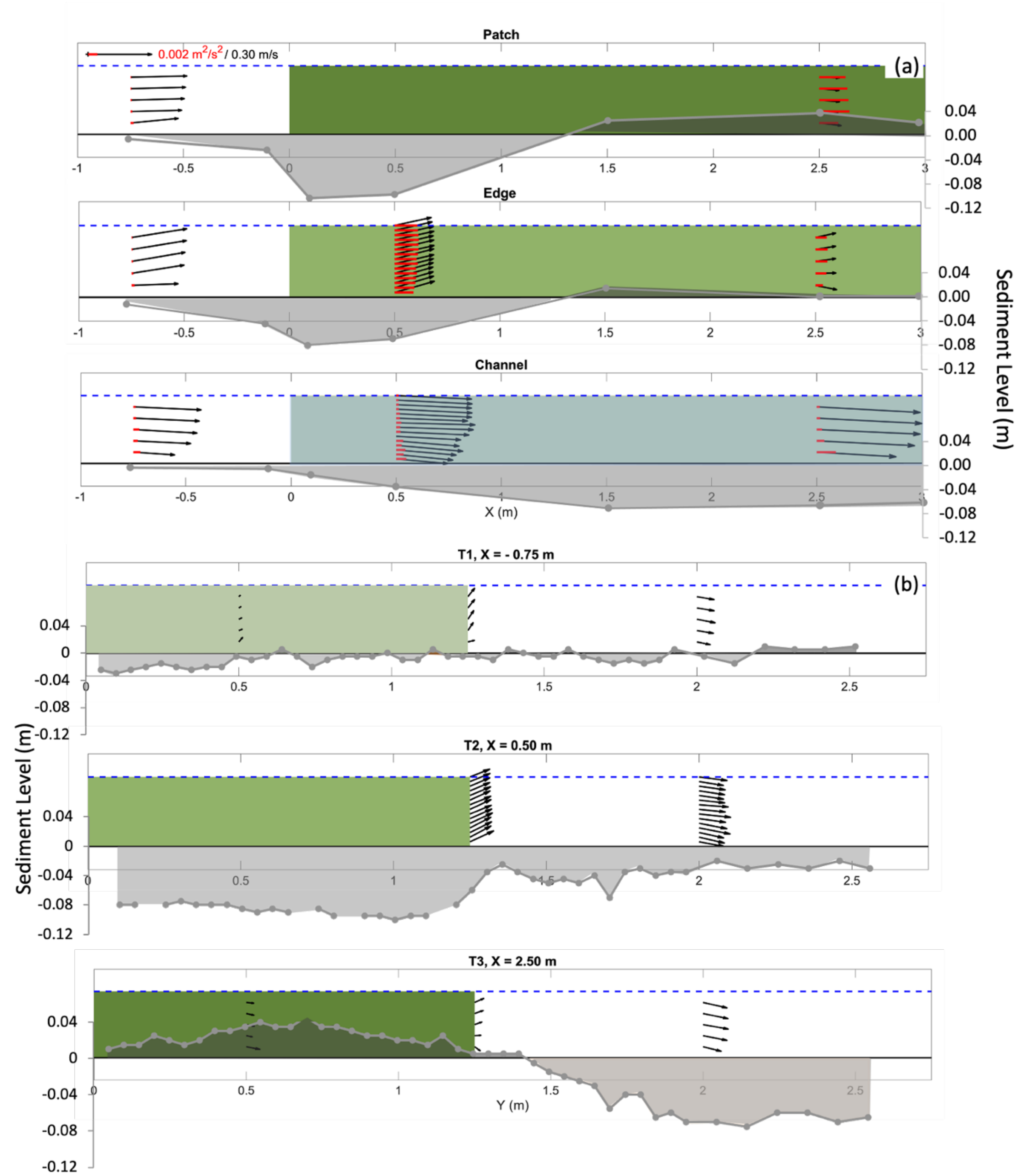

Figure 4. Velocity (black arrows), TKE magnitude (red lines) and sediment elevation (grey lines) for rigid vegetation and CC (currents only): a) longitudinal sections (inside the patch Y = 0.625 m, dark green, at the lateral edge Y = 1.25 m, light green, and at the channel Y = 2.00 m, blue) and (b) cross sections (at T1 X = -0.75 m, T2 X = 0.50 m, and T3 X = 2.50 m). Panel (a) displays velocity profiles obtained using X and Z components and (b) profiles considering Y

and Z components. Sediment erosion elevation is represented by light grey shading, whilst accumulation is dark grey shading. Water level (0.3 m) is presented by a dashed blue line.

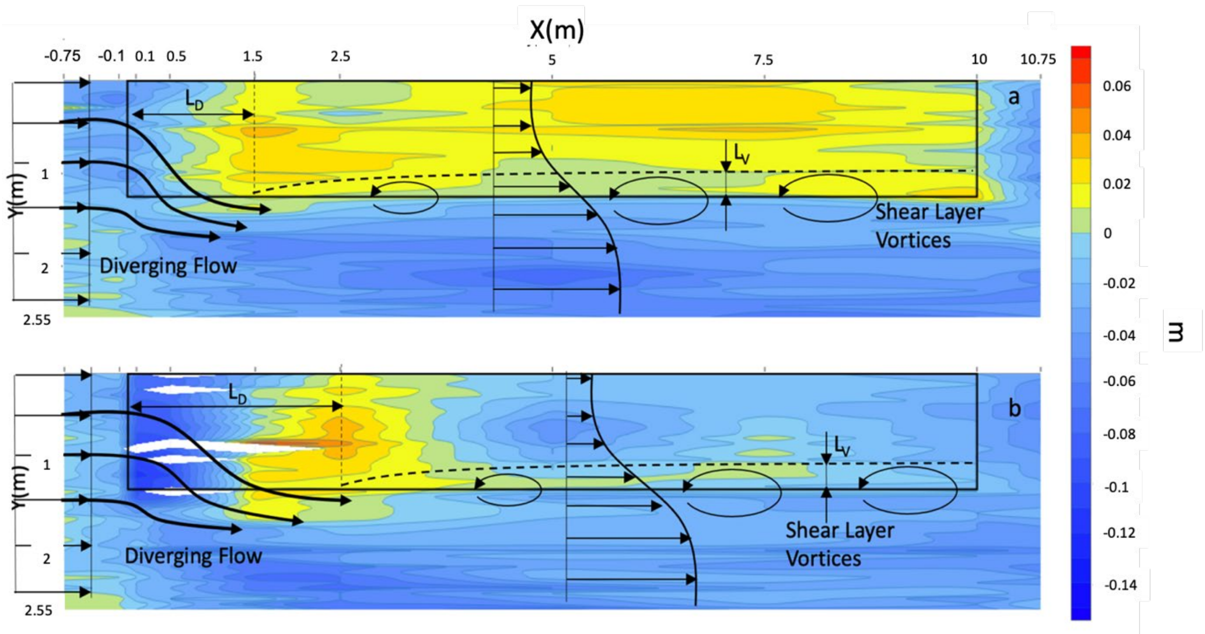

Figure 5. Top view of sediment elevation changes and conceptual sketch of the flow field near vegetation patches, flexible (a) and rigid (b). Warm colours represent sediment accumulation whereas cold colours display erosion. Flow diversion begins offshore of the patch and extends a distance L_D into the path. L_D indicates the end of the diverging flow and the beginning of the shear-layer development at the lateral edge of the patch. The shear-layer penetrates a distance L_V into the patch.

The conceptual sketch (Figure 5) for both vegetation patches shows the main differences in flow divergence and sediment movement. Stronger flow divergence by the rigid vegetation (panel b) produces a longer diverging flow region at the leading edge, L_D, and greater erosion in the channel due to the larger velocities observed for both patches at the leading edge. After the diverging flow region, there is a fully developed region within the rigid vegetation, where the velocity is uniform across the patch width and length. A shear layer forms at the interface between the patch and the lateral channel, where shear layer vortices develop. Since both patches present the same frontal area per volume, the length-scale of vortex penetration (L_V) is expected to be similar for both cases, being slightly bigger for the rigid vegetation due to its larger C_D value, as discussed above. Taking C_D = 1 gives a value for L_V of approximately 0.20 m.

Tanino and Nepf (2008)'s formula for turbulence generated by element wakes considered a balance between the production of TKE and its viscous dissipation. The formula shows that larger TKE values are obtained in cases with greater in-canopy velocities. At X= 2.5 m, TKE in the flexible vegetation has a mean value of 0.001 m^2/s^2 while for rigid vegetation has a mean TKE of 0.006 m^2/s^2, whilst ϕ is equal to 0.012 and 0.060 for flexible and rigid vegetation, respectively. Whereas the depth averaged velocity at X = 2.5 m is equal to 0.155 m/s (0.0016) for flexible and 0.097 m/s (4e^{-06}) for rigid vegetation (values in brackets show the standard deviation). Thus, the greatest TKE produced by element wakes is found in the rigid vegetation (Figure 4 (a), top panel), despite the smaller in-canopy velocity. Following the formular from Tanino and Nepf (2008), this indicates larger TKE for the rigid vegetation than for the flexible one, confirming, the greater influence of ϕ versus the velocity reduction in terms of TKE produced by element wakes. Turbulence can also be generated within shear regions, such as at patches' lateral edges. This process is observed in the flexible vegetation case, where the largest TKE values are recorded at the lateral edge of the patch (Figure 3 (a)).

At the end of the diverging flow region in the rigid vegetation, sediment deposition increases in the along-channel direction as the local velocity decreases. The opposite occurs in the fully developed flow region, where deposition decreases longitudinally through the patch, as the sediment concentration in the water column is depleted. In this region, sediment elevation is almost uniform across the patch width, except within the shear layer region.

Turbulent transport is enhanced by shear layer vortices, which transport resuspended sediment along the lateral edge of the patch. This transportation results in an accumulation of sediment at the downstream side edge of the flexible vegetation patch and causes some of the sediment that has been suspended in the diverging flow region of the rigid vegetation to be deposited at the lateral edge (Figure 5).

3.2 Wave only runs

Wave height evolution was measured in the high-density vegetation patches and is shown in Figure 6 combined with the sediment elevation measured along the centerlines.

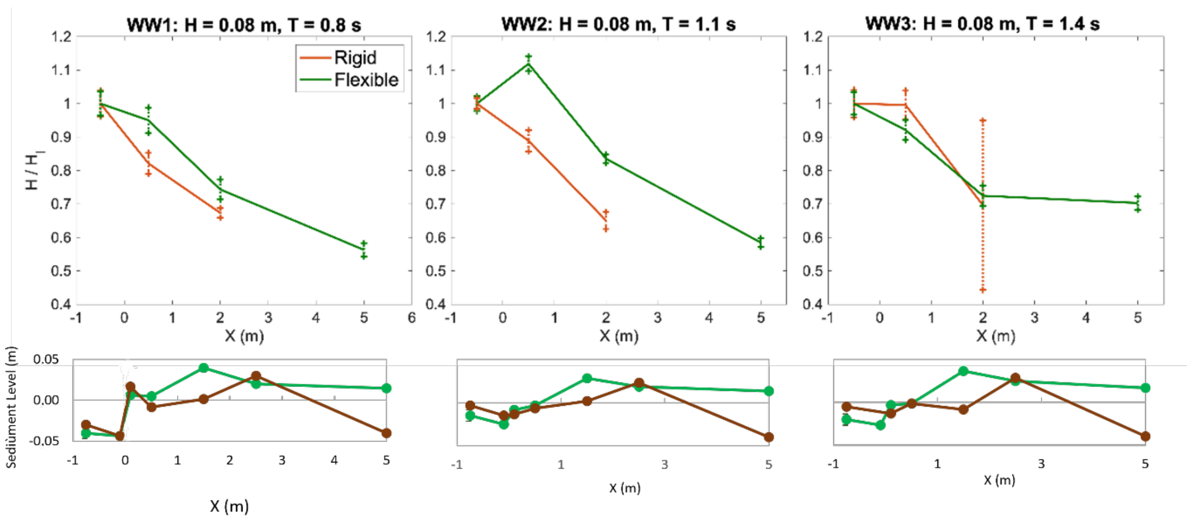

Figure 6. The top three panels show relative wave height (H/H_I) evolution along the two high density patches, rigid (brown) and flexible (green). The bottom three panels show the sediment level changes within the patches at the same Y-position (Y = 0.625 m). WW1 (wave period 0.8 s) is shown in panel (a), WW2 (wave period 1.1 s) in panel (b) and WW3 (wave period 1.4 s) in panel (c). Crosses (top panels), dashes (bottom panels) and dotted lines represent standard deviations (+/-). See Table 1 for incident wave characteristics in each case.

Free surface measurements at X = 5 m were not recorded for the rigid vegetation run. However, the results show that the flexible vegetation did not reduce the wave height as much as the rigid vegetation which reduced the wave height up to 23% more than the flexible vegetation at X = 2 m (Figure 6). This difference is also shown by greater velocities within the patch at X = 2.5 m for flexible vegetation compared to rigid vegetation (Figure S3, S4 and S5). There is similar wave height attenuation for the three tested wave conditions, with a small decrease in the amount of attenuation with increasing wave period (Figure 6). The mean values and standard deviations (in brackets) of the relative wave heights at X = 2 m are 0.77 m (0.06 m) and 0.67 m (0.02 m) for the flexible and rigid vegetation, respectively, and 0.62 m (0.07 m) for the flexible vegetation at X = 5 m. Thus, it is observed that the flexible vegetation needs more than twice the distance from the leading edge than the rigid vegetation to obtain similar wave height attenuation, although it should be noted that the largest rate is observed for the first 2 m of vegetation in both cases. This is further confirmed by the velocities recorded in both patches, which are reduced by more than 30% after 2.5 m in both cases (Figures S3, S4 and S5). The greatest TKE values are observed for the rigid vegetation, but TKE is reduced by up to 40% from 0.5 to 2.5 m in all wave cases in both patches.

At the leading edge, where velocities have not yet been attenuated, sediment is transported into the patch. The decrease in velocity and TKE leads to sediment deposition downstream of the leading edge in both vegetation mimics at 1.5 - 2.5 m (bottom panels in Figure 6). Sediment deposition and consequently sediment accumulation occurs over a shorter distance in the flexible vegetation patch (at 1.5 m) compared to the rigid vegetation patch (at 2.5 m) (Figure 6). Within the patch, the largest accumulation for flexible vegetation occurs at 1.5 m, while for rigid vegetation it is observed at 2.5 m (Figure 6). Sediment erosion at the leading edge is milder for the flexible vegetation which may be due to the greater turbulence produced around the rigid elements, which resuspends a larger amount of sediment compared to the flexible vegetation case (Figure 6).

3.3 Waves and Currents

The interactions of waves and currents with both types of vegetation, at both densities (high and low), is presented in this section. For low densities the flow is diverted less compared to high densities, so it penetrates further into the patch with fewer stems and greater velocities are recorded at X = 0.5 – 2.5 m. However, high densities reduce velocity within the patch more strongly than low densities. For flexible vegetation, the velocity decreases from 20 to 24% (low density cases) and 20 to 40% (high density cases) with the smallest reduction for the longest wave period and the largest for the shortest (Figures 6, S6 (a) and S7 (a)). In the case of rigid vegetation, the decrease in velocity between X = 0.5 and 2.5 m is smaller, from 2 to 22%, with the smaller values observed for low-density cases. The velocities at X = 0.5 m are already lower than those recorded for the flexible vegetation due to the greater divergence of the flow at the leading edge. The velocities for the low-density cases are greater than those for the high-density ones (Figure 7).

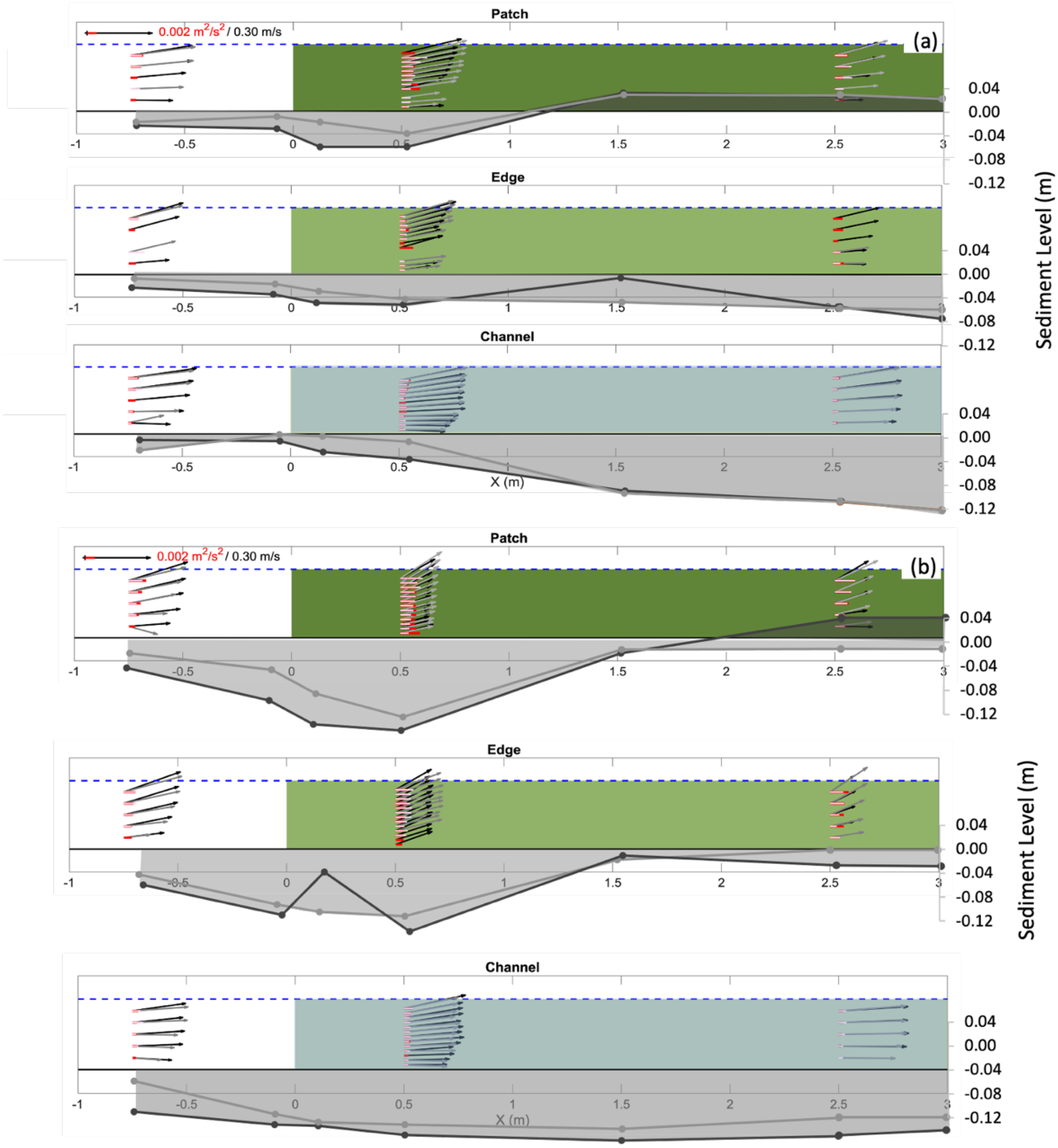

Figure 7. Velocity profiles using X and Z velocity components, TKE magnitude and sediment elevation for flexible vegetation (panel (a)) and rigid vegetation (panel (b)). Panels (a) and (b) display longitudinal sections (inside the patch, dark green, at the lateral edge, light green, and at the channel, blue). Black arrows and red lines display velocity and TKE for high-density. Grey arrows and light pink lines result for low density. Dark grey lines display sediment elevation results for high density and light grey lines for low density. Water level (0.3 m) is presented by a dashed blue line.

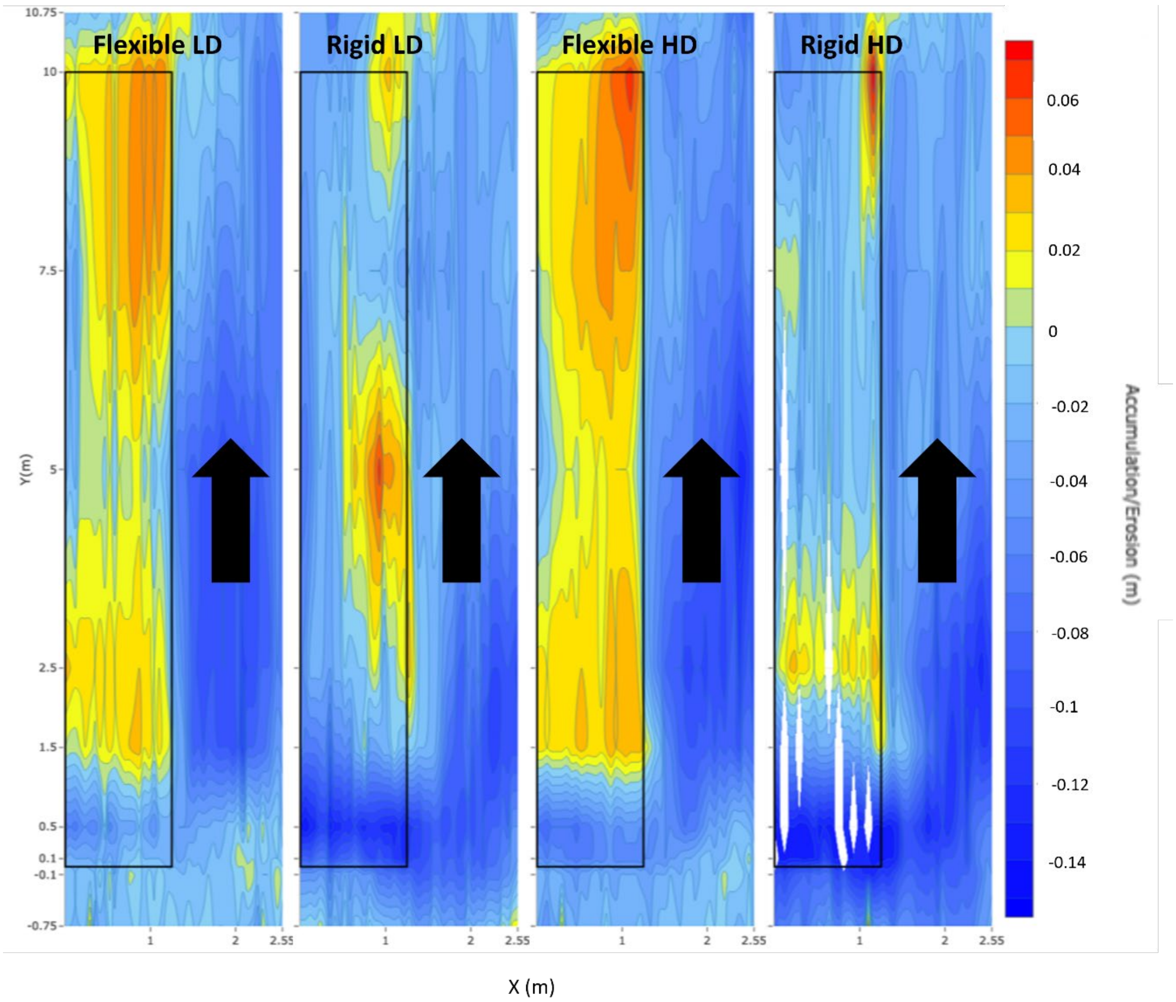

Figure 8. Top views of the whole test section for low- and high-density tests in flexible and rigid mimics for combined waves and flow. Colours show sediment accumulation (in warm colours) and erosion (in cold colours) and black arrow the main flow direction. The vegetation patches are shown by a black square.

Longer wave periods lead to greater TKE values within the patch for both vegetation types and densities. For the flexible vegetation TKE does not decrease in the first 2.5 m for the low-density cases, especially for longer wave periods where TKE increases from X = 0.5 to 2.5 m by up to 22% (Figure 7). At high-density cases, TKE decreases from X = 0.5 to X = 2.5 m for all three waves and current conditions (Figure 7, S6 (a) and S7 (a)). TKE values recorded for rigid vegetation at both densities are greater than values recorded for flexible vegetation. For rigid vegetation at X = 0.5 m within the canopy, TKE values found for high-density (Figure 7(b)) are larger than the values for low-density, especially near the bottom (i.e., from the bottom to about half the water depth). This larger turbulence near to the bottom for the high-density cases increases sediment resuspension at the leading edge, which leads to greater levels of erosion (Figure 7 and 8). At X = 2.5 m, TKE decreases for the high-density cases, and sediment deposition is observed. However, for the low-density cases, the TKE does not significantly decrease within the patch from X = 0.5 to 2.5 m (Figures 7 (b), S5 (b) and S6 (b)) leading to increased sediment transport resulting in a sediment deposition zone further into the patch (around X = 5 m). Thus, a change in plant density leads to a change in the longitudinal deposition of sediment within the rigid vegetation patch, with sediment deposition at a greater distance from the leading edge for lower densities. Therefore, for rigid vegetation, both turbulence intensity and flow velocities determine sediment transport in and around the patch. It is also shown that a decrease in vegetation density leads to less erosion along the channel, due to the gentler divergence of the flow, and to a larger area within the patch from the leading edge where sediment is eroded.

3.4 Scale-dependent feedback

Following Bouma et al. (2013) the scale-dependent feedback is analysed in this section by using flow deceleration within the patch as a proxy for the positive feedback and flow acceleration around the patch as proxy for the negative feedback (discussed in the next section in detail). The scale-dependent feedback is evaluated for the current-only and waves-and-currents cases at two longitudinal positions: X = 0.5 and 2.5 m. Figure 9 shows the scale-dependent feedback strengths for both positions, rigid and flexible vegetation, and the different hydrodynamic conditions.

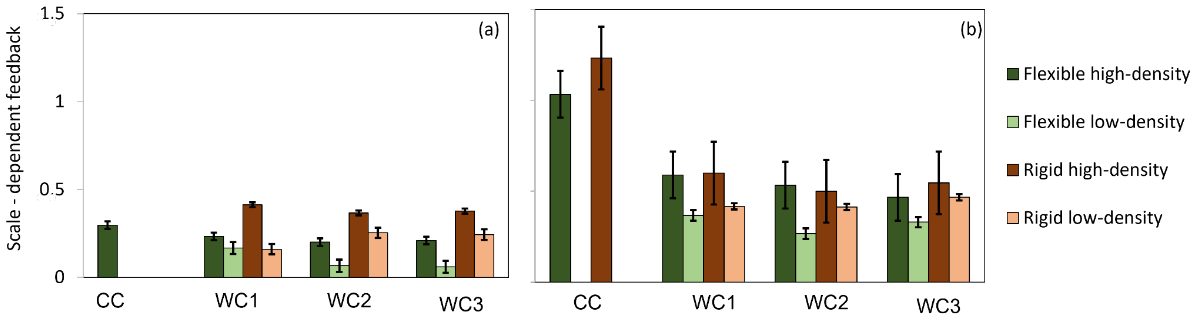

Figure 9. Scale-dependent feedback observed for (a) transect 2, X = 0.5m, and (b) transect 3, X = 2.5 m, and high- and low-density vegetations (flexible and rigid) under CC, WC1, WC2 and WC3 hydrodynamic conditions (see Table 1).

Figure 9 shows that the scale-dependent feedback increases when moving towards the patch from the leading edge in agreement with the velocity decrease produced by the canopy. Figure 9 (b), X = 2.5 m, shows larger values than Figure 9 (a), X = 0.5 m, for all hydrodynamic and vegetation conditions, especially for CC, at least for flexible vegetation since no measurements at X = 0.5 m are available for the rigid one.

At the leading edge, (Figure 9 (a)), and for high-density cases, the scale-dependent feedback is almost constant for both vegetation types, being equal to 0.24 (0.04) for flexible vegetation and equal to 0.39 (0.02) for rigid vegetation. This difference is also observed for the low-density cases, where the mean value for the flexible vegetation is equal to 0.10 (0.06), while it is 0.22 (0.05) for the rigid vegetation. For flexible vegetation, a decrease in the scale-dependent feedback is observed with increasing wave periods, especially for low-density cases. This decrease may be linked to the ability of flexible vegetation to move and reconfigure under the flow action. Finally, it is observed that the scale-dependent feedbacks for low density cases are 42 and 57% smaller than those for high-density cases for flexible and rigid vegetation, respectively. Thus, the strong flow divergence produced by high-density cases (with = 0.012 and 0.060, for flexible and rigid vegetation) is significantly reduced by half.

At X = 2.5 m, (Figure 9 (b)), for low-density cases, the scale-dependent feedback is greater than the value for high-density at X = 0.5 m, confirming that for low-density cases a longer distance inside the patch is needed to achieve the same velocity attenuation. In contrast with what is observed at X = 0.5 m, for wave and currents conditions and high-density cases, similar scale-dependent feedbacks are found for rigid and flexible vegetation, being equal to 0.55 (0.05) and 0.53 (0.06), respectively. For low densities with smaller ϕ, a significant difference in the value of the scale-dependent feedback is still observed between rigid and flexible vegetation at X = 2.5 m, with values equal to 0.43 (0.03) and 0.32 (0.05), respectively. Thus, it is found that dense flexible canopies may be very effective at attenuating flow velocity over short distances, but once the density of the canopy is significantly reduced (by half in this case) the attenuation of the meadow is more limited. However, for rigid vegetation, the same density change, i.e., a ϕ change, does not result in such a large loss of attenuation capacity of the canopy.

4. Discussion

Ecosystem engineers' traits affect hydrodynamics and sediment dynamics. Our results show that flexible and rigid vegetation reduced flow speed by 50% and 70%, respectively, for unidirectional flow (Figure 3 and 4). Within this unidirectional flow, turbulent kinetic energy was generally lower in the flexible vegetation (0.001 m^2s^{-2}) compared to the rigid vegetation (0.006 m^2s^{-2}) which corresponds to greater erosion (Figure 3 and 4). Under wave-only conditions, the flexible vegetation attenuated waves slower initially than rigid vegetation. The flexible vegetation required more than twice the distance from the leading edge than the rigid vegetation to obtain similar attenuation rates (Figure 6). However, by 2.5 m both vegetation types reduced turbulent kinetic energy by 40% under only wave conditions, which led to sediment deposition after the leading edge for both vegetation mimics at 1.5-2.5 m (Figure 6). For flexible low-density vegetation under combined waves and currents, the flow speed reduction within the patch ranged from 20-24%, whilst for high density it was 20-40%, the change in flow speed corresponded to larger sediment accumulation in high density flexible plants, which occurred closer to the leading edge (Figure 7). In the case of the rigid vegetation, the decrease of flow speed within the patch ranged from 2-22%, with the smaller values observed for low-density vegetation. Combining waves and currents resulted in increased channel speeds when the current first encountered the vegetation across all conditions, for both patches at high density. TKE values recorded for flexible vegetation at both densities were lower than those recorded for rigid vegetation, as shown for current-only tests. Larger TKE values indicated greater sediment erosion at the front of the rigid vegetation (Figure 8). The biggest increase in scale dependent feedback was found between 0.5 and 2.5 m in flexible vegetation marsh patches under all wave and current conditions. However, generally, scale-dependent feedback was greater in the rigid vegetation, especially at lower densities.

4.1 Effects of flexible vegetation

In terms of the ability to reduce erosion and accumulate sediment, flexible vegetation clearly has advantages. In flexible vegetation the formation of a sharp precipice does not occur due to the strong erosion at the front of the patch, which forms in the rigid vegetation (Figure 3, 4 and 7). Previous research has found most of the suspended particles transported within flexible canopies collide with the moving flexible stems leading to particle capture by loss of momentum (Ganthy et al., 2015). The current study confirms this assessment, for example under wave-only conditions where the flexible vegetation caused no erosion (only accumulation), in contrast to the rigid vegetation (Figure 6). As noted in other studies (King et al., 2012; Nepf and Vivoni, 2000) turbulence was generated within the shear regions along the lateral edge of the flexible vegetation patch.

4.2 Effects of rigid vegetation

The rigid vegetation mimics had a greater effect in attenuating hydrodynamic energy compared to flexible vegetation for two reasons: firstly, the rigid vegetation does not bend and therefore has a greater flow resistance (Bouma et al., 2013, 2005). Secondly, there is larger drag caused by the rigid vegetation due to its rigidity and submerged solid volume fraction (Maza et al., 2019, 2015; Paul et al., 2012), as shown by the larger free surface gradient in the rigid vegetation under currents only, in agreement with (Bouma et al., 2009; Tanino and Nepf, 2008). The rigid vegetation's ability to quickly reduce momentum within the patch under all hydrodynamic conditions reduces its ability to accumulate sediment. This is because the reduction increases turbulence, which these results suggest is the dominant hydrodynamic process for erosion in rigid vegetation (Tinoco and Coco 2018). Under unidirectional flow and waves combined with currents, TKE was generated around the individual vegetation mimics, which was stronger for rigid vegetation compared to flexible vegetation (Tanino and Nepf, 2008). This can be linked to rigid mimic's traits such as rigidity and diameter. When exposed to strong hydrodynamic conditions, they generate intense near bed turbulence which causes local scouring around the base of the roots (Norris, 2021). Bouma et al. (2009) found that, for rigid vegetation, this process was mainly due to basal diameter, which determines the degree of scouring. Therefore, the larger diameter of rigid mimics leads to greater scouring which is linked to the overall larger erosion produced within the rigid vegetation. Additionally, near-bed coherent structures generated by rigid stem-bed-flow interactions (such as horseshoe vortices) can significantly alter the near-bed stresses locally in front of the rigid elements resulting in additional sediment resuspension (Schanderl et al., 2017b, 2017a). Previous research has established there is a relatively sheltered interior in rigid vegetation i.e., mangroves (Folkard, 2019; Norris, 2019) where deposition occurs. This study also located a sheltered interior, where the lowest turbulence resulted in the greatest deposition of sediment within rigid patches. Deposition generally occurred much further (ca. 2 m) into the rigid vegetation patch compared to the flexible vegetation patch (ca. 1 m).

The larger flow speed inside the lower density patches of rigid vegetation resulted in sediment being transported further into the patch. This is facilitated by the decrease in TKE in the first few meters of the patch for high density but not for low density (similar to the flexible vegetation cases) (Figure 7 (b)). This was shown by the sediment accumulation patterns, where accumulation was produced closer to the leading edge in the higher density patches (Figure 8).

4.3 Bio-physical feedbacks in flexible and rigid vegetation

Three possible feedback processes have been identified in this study: a positive feedback; a negative feedback; and the scale-dependent feedback. The positive feedback occurs where mimic vegetation attenuates flow energy to allow for sediment accumulation (Bouma et al., 2009, 2005; Gourgue et al., 2021). From this, we deduce that flexible vegetation will have stronger positive feedback compared to rigid vegetation, as flexible vegetation will accumulate more sediment in their patch compared to rigid vegetation under all the hydrodynamic conditions.

The negative feedback occurs where mimic vegetation deflects flow, causing greater channel erosion, in-situ this could reduce the vegetation's lateral expansion but is also a key element of channel formation and hence wetland drainage (Temmerman et al., 2007; Zong and Nepf, 2011). The rigid vegetation cases had greater channel erosion under unidirectional flow, due to stronger flow diversion compared to the flexible vegetation case. When considering combined waves and currents, this study shows that rigid vegetation (at both densities studied) was also more likely to develop a negative feedback of channel formation, as diversion of the current was greater. The stronger flow divergence relates to the fact that, although both patches present the same frontal area, rigid emergent elements produce greater flow resistance than flexible, nearly emergent ones, as reported previously (Bouma et al., 2013, 2005). Previous studies have also found that higher densities cause greater flow deflection which results in more pronounced channel erosion. Whilst lower vegetation density allows the flow to dissipate within the vegetation (due to there being more space around the vegetation roots or stems), therefore less channel erosion (Gourgue et al., 2021). The front of the lower density flexible vegetation had less channel erosion compared to the higher density case in agreement with previous studies where flow passed through flexible vegetation and was not deflected as strongly (Bouma et al., 2013, 2009). This deflection indicated a weaker manifestation of negative feedback i.e., channel erosion, as decreasing density reduces deflection by flexible vegetation at this point (Figure 8). Additionally, along the leading edge of the high-density flexible vegetation patch, erosion from deflection is reduced with decreasing flow speeds. The depth of erosion in the channel was dependent on the density of the plants and the hydrodynamic regime (Folkard, 2019). The absence of these negative feedbacks in low flow environments may facilitate formation of flexible patches without erosion troughs and could facilitate expansion of such vegetation as is commonly observed in calmer hydrodynamic areas (Bouma et al., 2009). Conversely, at larger velocities and higher densities, increased channel depth could in -situ reduce the plants' success in expanding laterally into the channel.

The scale-dependent feedback concerns the ratio of the flow speed within the vegetation to that in the channel. Changes in ratios between the rigid and flexible patch indicates flexible dense vegetation was effective in attenuating flow speed, but once patch density was significantly reduced, the attenuation capacity of the patch was limited. However, for rigid vegetation the same density change does not result in such a large loss of attenuation capacity of the meadow. The values obtained at X = 2.5 m in the currents only cases agree with values reported by Bouma et al. (2013), despite the differences between the tested vegetation (real vegetation in the case of Bouma et al. 2013 while mimics are used here). The value for rigid vegetation (1.23), is close to that obtained for *Spartina anglica* (~1.20, Figure 5 in (Bouma et al., 2013), a rather rigid species, while the value obtained for flexible vegetation (1.03), is close to that obtained for *Salicornia procumbens* (~0.90, Figure 5 in Bouma et al. 2013), a more flexible species.

Additionally, this study found that multi-scale feedbacks are also associated with community and plant traits such as density of vegetation and rigidity/flexibility of the plant. Recent studies have also shown the importance of traits (Temmink et al. 2020) for plant establishment. However, there are a variety of traits associated with salt marsh and mangrove plants and their ecosystems and further research should concentrate on identifying potential abiotic boundary conditions determining hydrodynamic buffering and sediment transport capacity. Sediment accumulation is crucial for salt marsh and mangrove survival, this research increases our understanding of bio-physical limitations to lateral expansion of these ecosystems. However, for these ecosystems to maintain their role as a coastal defence in the context of climate-change induced sea-level rise, we require further information (i.e., community and plant traits) to allow prediction of expansion with changing external forcing. This information will become more important for designing ecosystem-based coastal protection measures that are climate resilient.

4.4 Application to natural environments

Our results present insights into the effects of vegetation flexibility and density on sediment dynamics, however, their transfer to natural conditions may be partially limited by the simplifications introduced while constructing the vegetation mimics. While the rigid mimics model mangrove prop roots reasonably well with respect to individual (diameter, length) and community (density) traits as well as rigidity, the flexible mimics neglect the effect of leaves on vegetation drag. Previous work has highlighted the importance of leaves and their reconfiguration under hydrodynamic loading for vegetation drag (San Juan et al. 2019; Whittaker et al. 2015; Schoneboom and Aberle 2009) and instantaneous flow fields (Tinoco et al. 2020). However, resulting turbulent flow is most prominent in the upper part of the canopy while the region close to the bed is less affected (Tinoco et al. 2020). Especially for flexible coastal wetland vegetation (e.g. salt marshes) this pattern coincides with standing biomass distribution. Close to the bed, most salt marsh plants exhibit individual stems growing from the roots with branches and leaves only occurring higher up along the plant. As sediment dynamics will be governed by the local flow near the bed rather than fluctuations at the top of the canopy, leaves play a minor role in this context. They do, however, complicate calculations of the frontal area due to their constant changes in position such as streamlining under approaching flow (Aberle and Järvelä 2015). We thus decided on a flexible vegetation model which models vegetation shape close to the bed and at the same time allows for a constant frontal area per canopy volume for comparison with the stiff mimics. Consequently, our results based on mimics provide insights into the general sediment dynamics at leading and lateral edges of coastal wetland with flexible (salt marsh) and rigid (mangrove) vegetation, while the application of results on the flow field higher up in the water column may be limited.'

5. Conclusions

This paper highlights the differences observed between two mimic ecosystem engineers (mangrove trees and salt marsh plants) with different characteristics, which are subjected to the same hydrodynamic conditions. The hydrodynamic and sedimentation processes identified for both ecosystems are linked to different feedbacks. A positive feedback was identified in which vegetation attenuates hydrodynamic energy allowing sediment accumulation within the patch and a negative feedback associated with the high velocities, produced from flow divergence, causing channel erosion. Greater channel erosion could compromise the lateral expansion of the vegetation. High rigid vegetation densities enhance this negative feedback. Lower flexible vegetation densities combined with calmer hydrodynamic conditions could facilitate the expansion of flexible patches as these patches have less flow divergence and therefore less channel erosion. The strong flow divergence from rigid vegetation highlights their importance for buffering hydrodynamics but at the cost of potentially increased erosion within the frontal patch and lateral edges. These findings illustrate the spatial dimensions of the ecosystem engineering outcome of two contrasting intertidal wetland species.

6. Acknowledgments

This study (H+DHI-10-HyWEdges) received funding from European Union, Hydralab+. The authors would like to thank DHI for the use of their total environmental stimulator flume and the support staff. M. Maza is sincerely grateful to the Spanish Ministry of Science and Innovation for the funding provided in the grant RTI2018-097014-B-I00 of Proyectos de I+D+i Retos Investigación 2018 funded by MCIN/AEI/10.13039/501100011033 and by "ERDF A way of making Europe".

7. Appendices

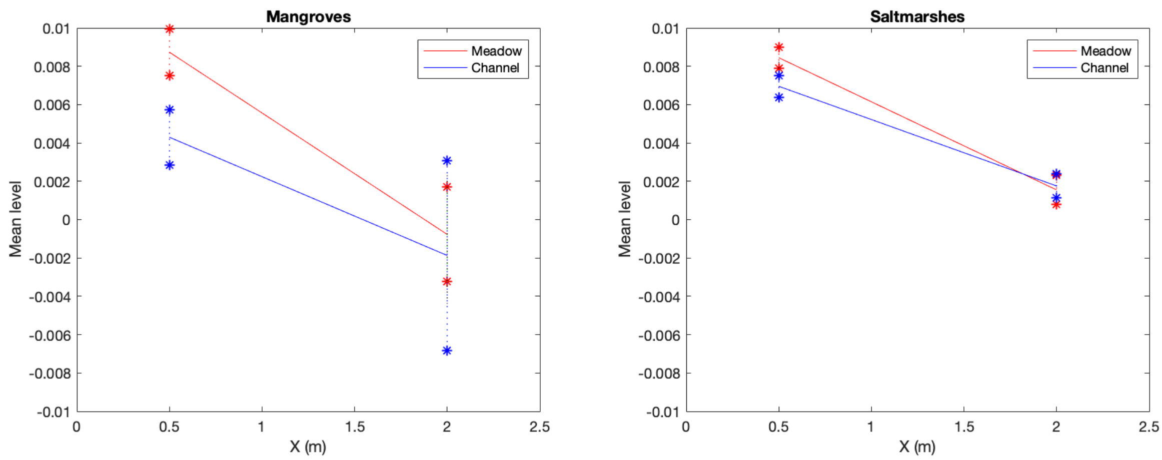

Figure S1. Free surface elevation inside the rigid and flexible vegetation. Red lines show results inside the vegetation field and blue lines values at the channel. The standard deviation of the data is shown by stars.

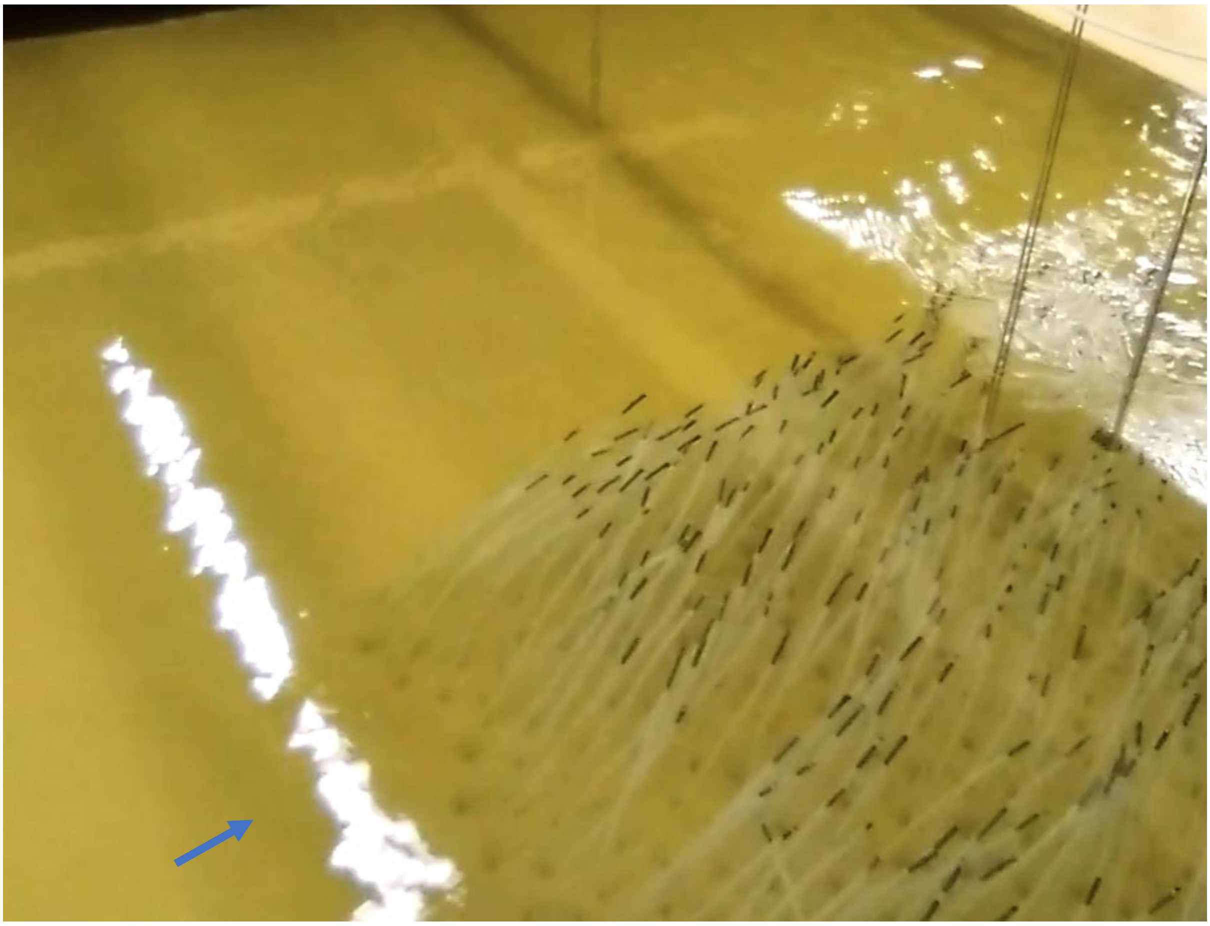

Figure S2. View of the leading edge of the flexible mimic field under unidirectional flow conditions (the blue arrow shows the flow direction). Plants reconfiguration under the flow action can be observed.

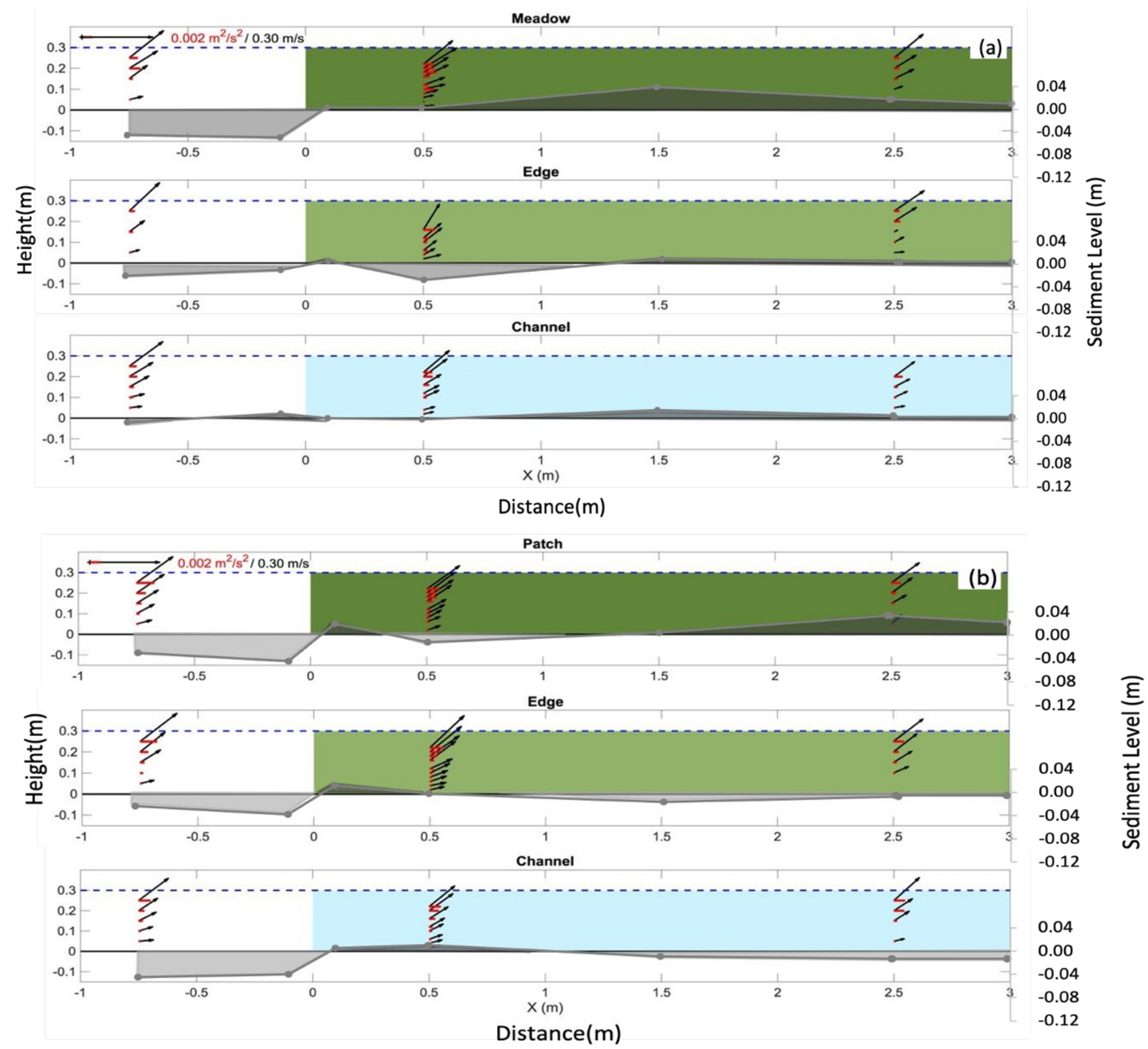

Figure S3. Velocity profiles using X and Z velocity components (black arrows), TKE magnitude (red lines) and sediment elevation (brown lines) for WW1 test and a) flexible and b) rigid vegetation. Longitudinal sections (inside the patch, dark green, at the lateral edge, light green, and at the channel, blue). Sediment erosion is represented by light brown shading, whilst accumulation is dark brown shading. Water level (0.3 m) is presented by a dashed blue line.

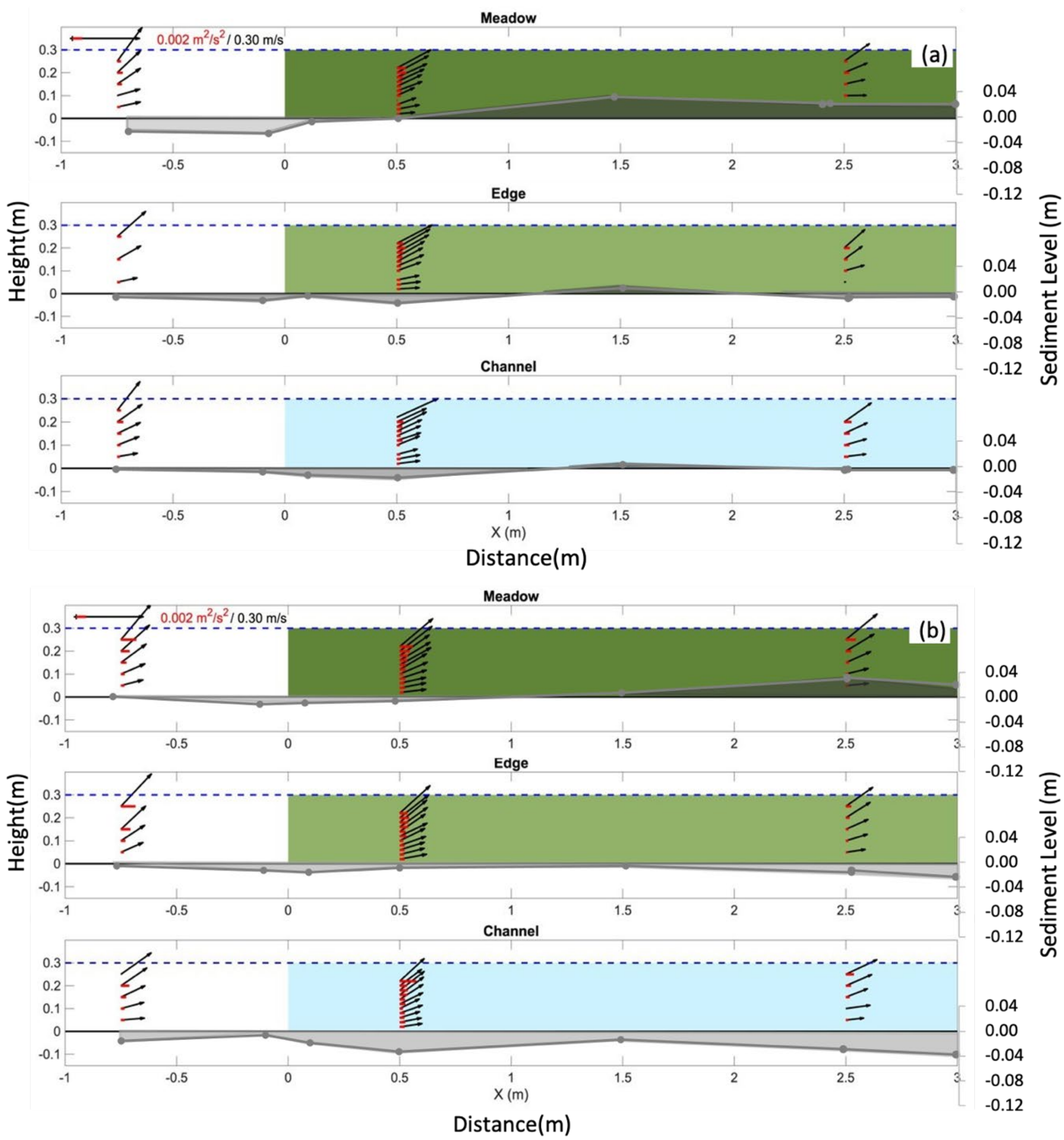

Figure S4. Velocity profiles using X and Z velocity components (black arrows), TKE magnitude (red lines) and sediment elevation (brown lines) for WW2 test and a) flexible and b) rigid vegetation. Longitudinal sections (inside the patch, dark green, at the lateral edge, light green, and at the channel, blue). Sediment erosion is represented by light brown shading, whilst accumulation is dark brown shading. Water level (0.3 m) is presented by a dashed blue line.

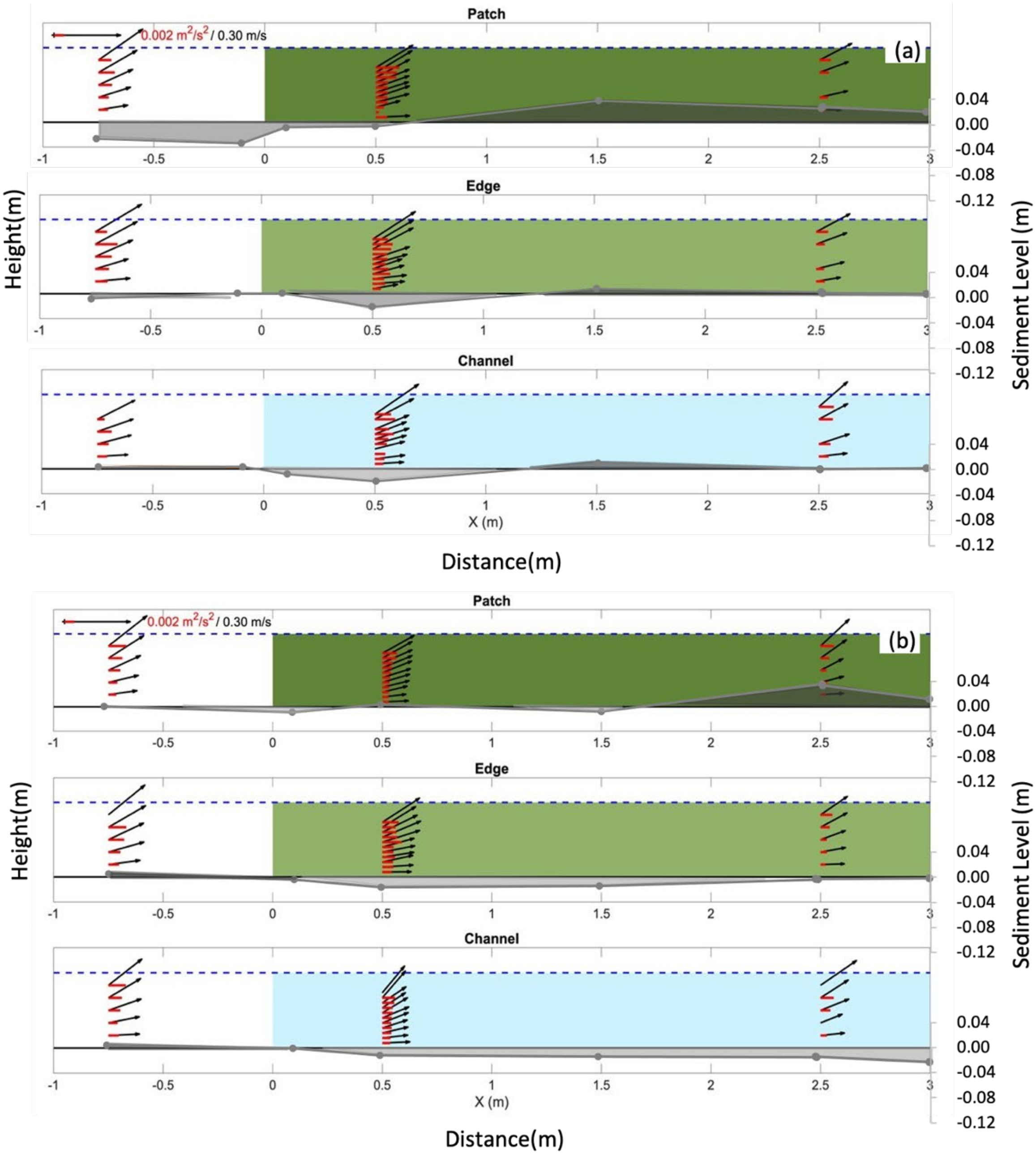

Figure S5. Velocity profiles using X and Z velocity components (black arrows), TKE magnitude (red lines) and sediment elevation (brown lines) for WW3 test and a) flexible and b) rigid vegetation. Longitudinal sections (inside the patch, dark green, at the lateral edge, light green, and at the channel, blue). Sediment erosion is represented by light brown shading, whilst accumulation is dark brown shading. Water level (0.3 m) is presented by a dashed blue line.

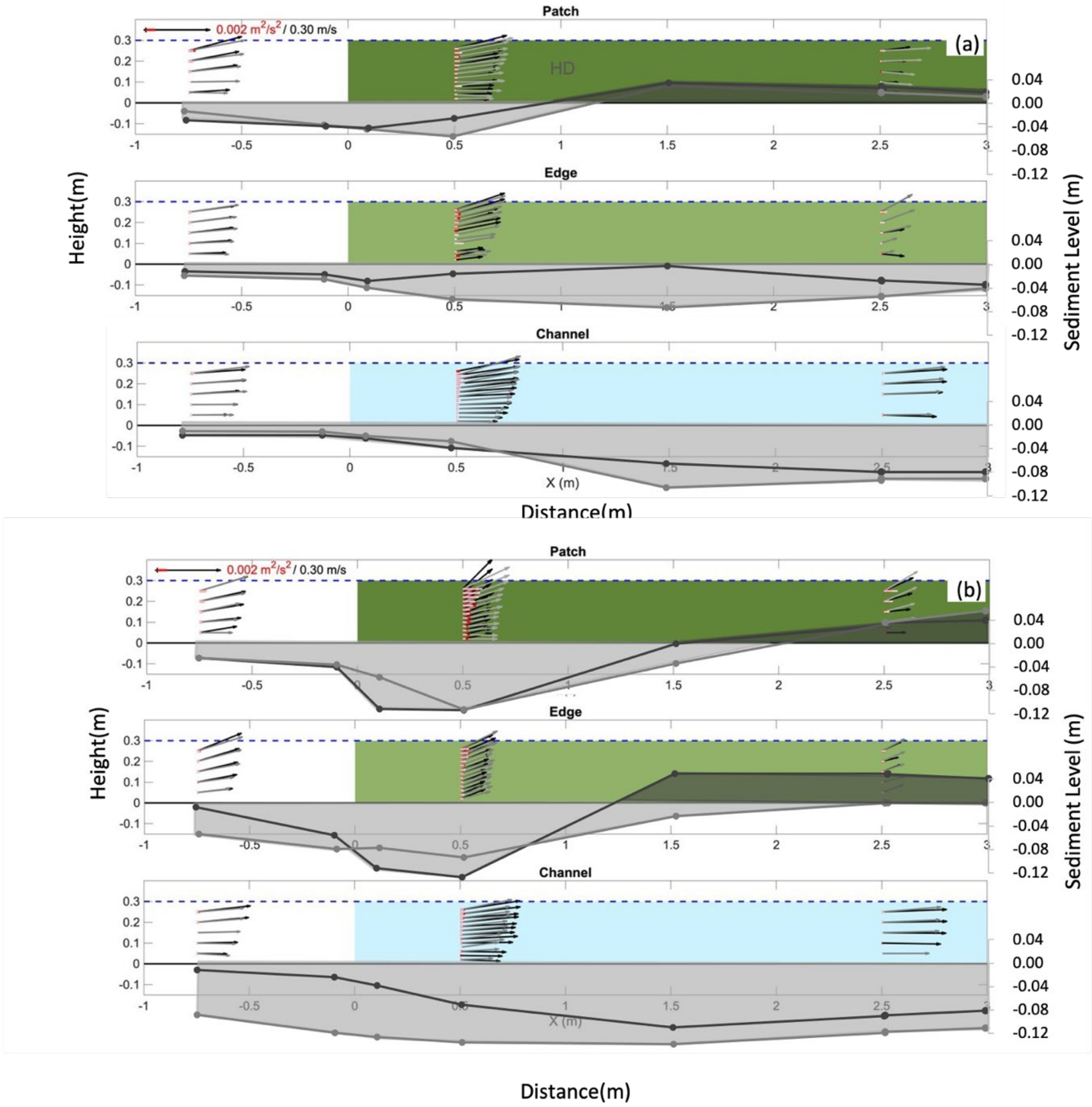

Figure S6. Velocity profiles using X and Z velocity components, TKE magnitude and sediment elevation for WC1 and flexible (panel (a)) and rigid (panel (b)) vegetation. Longitudinal sections (inside the patch, dark green, at the lateral edge, light green, and at the channel, blue). Black arrows and red lines display velocity and TKE for high-density. Grey arrows and light pink lines result for low density. Brown lines display sediment elevation results for high density and orange lines for low density. Water level (0.3 m) is presented by a dashed blue line.

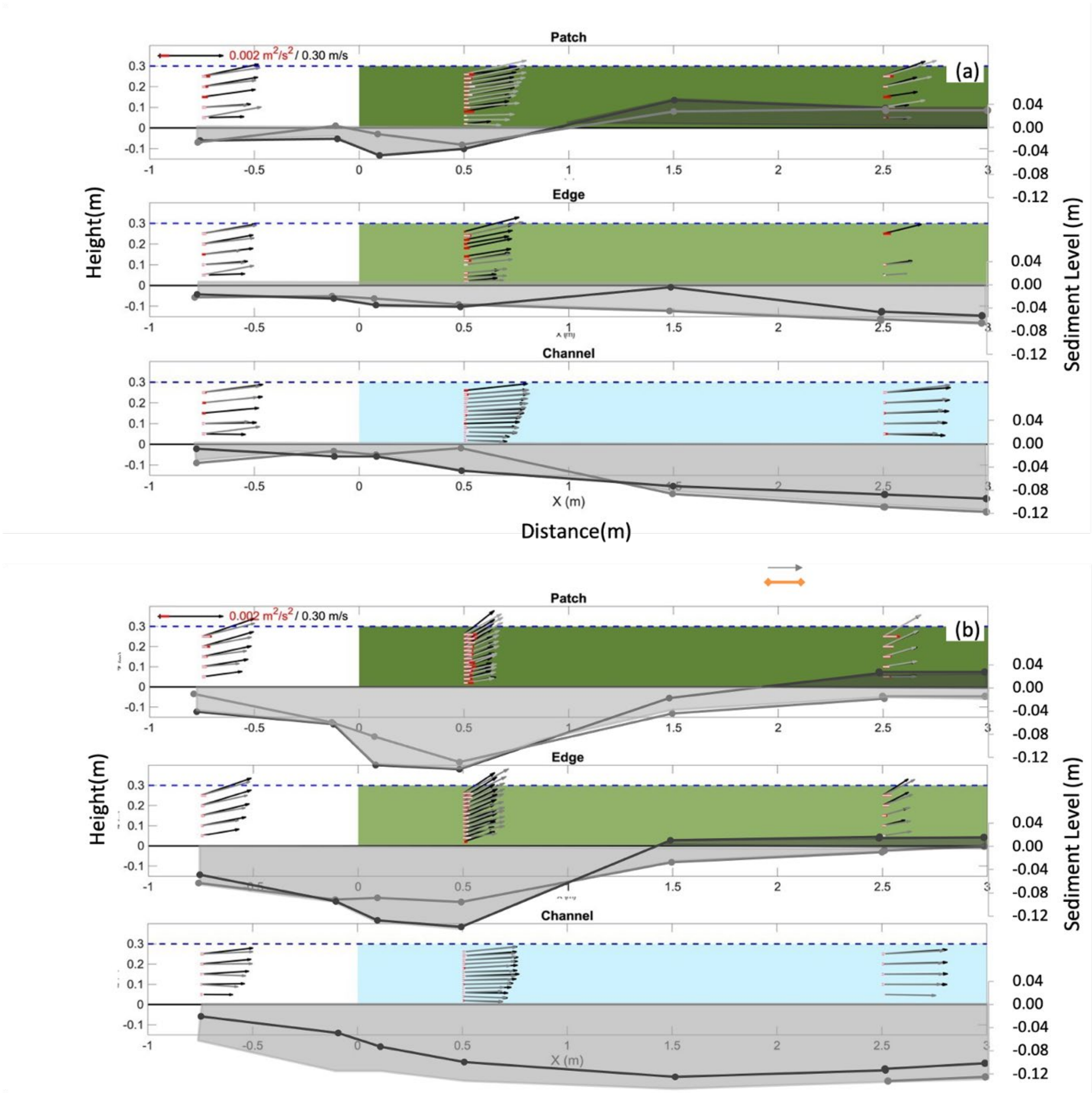

Figure S7. Velocity profiles using X and Z velocity components, TKE magnitude and sediment elevation for WC2 and flexible (panel (a)) and rigid (panel (b)) vegetation. Longitudinal sections (inside the patch, dark green, at the lateral edge, light green, and at the channel, blue). Black arrows and red lines display velocity and TKE for high-density. Grey arrows and light pink lines result for low density. Brown lines display sediment elevation results for high density and orange lines for low density. Water level (0.3 m) is presented by a dashed blue line.

8. References

Aberle, J., and Järvelä, J., 2015. "Hydrodynamics of Vegetated Channels," in Rivers -- physical, fluvial and environmental processes, eds. P. M. Rowiński, and A. Radecki-Pawlik (Cham: Springer), 519–541. https://doi.org/10.1007/978-3-319-17719-9

Balke, T., Herman, P.M.J., Bouma, T.J., 2014. Critical transitions in disturbance-driven ecosystems: identifying Windows of Opportunity for recovery. J Ecol 102, 700–708. https://doi.org/10.1111/1365-2745.12241

Barbier, E.B., 2007. Valuing Ecosystem Services as Productive Inputs. Economic Policy 22, 177–229. https://doi.org/10.1111/j.1468-0327.2007.00174.x

Bouma, T.J., De Vries, M.B., Low, E., Peralta, G., Tánczos, I.C., van de Koppel, J., Herman, P.M.J., 2005. Trade-offs related to ecosystem engineering: A case study on stiffness of emerging macrophytes. Ecology 86, 2187–2199. https://doi.org/10.1890/04-1588

Bouma, T.J., Friedrichs, M., van Wesenbeeck, B.K., Temmerman, S., Graf, G., Herman, P.M.J., 2009. Density-dependent linkage of scale-dependent feedbacks: a flume study on the intertidal macrophyte *Spartina anglica*. Oikos 118, 260–268. https://doi.org/10.1111/j.1600-0706.2008.16892.x

Bouma, T.J., Temmerman, S., van Duren, L.A., Martini, E., Vandenbruwaene, W., Callaghan, D.P., Balke, T., Biermans, G., Klaassen, P.C., van Steeg, P., Dekker, F., van de Koppel, J., de Vries, M.B., Herman, P.M.J., 2013. Organism traits determine the strength of scale-dependent bio-geomorphic feedbacks: A flume study on three intertidal plant species. Geomorphology 180–181, 57–65. https://doi.org/10.1016/j.geomorph.2012.09.005

Bouma, T.J., van Duren, L.A., Temmerman, S., Claverie, T., Blanco-Garcia, A., Ysebaert, T., Herman, P.M.J., 2007. Spatial flow and sedimentation patterns within patches of epibenthic structures: Combining field, flume and modelling experiments. Continental Shelf Research 27, 1020–1045. https://doi.org/10.1016/j.csr.2005.12.019

Brinkman, R., 2007. Wave Attenuation in Mangrove Forests: An Investigation Through Field and Theoretical Studies (PhD). James Cook, Douglas, Australia.

Cheong, S.-M., Silliman, B., Wong, P.P., van Wesenbeeck, B., Kim, C.-K., Guannel, G., 2013. Coastal adaptation with ecological engineering. Nature Clim Change 3, 787–791. https://doi.org/10.1038/nclimate1854

Eadie, R. W. IV and J. B. Herbich (1986). Scour about a single, cylindrical pile due to combined random waves and current. Proc. 20th Coastal Engineering Conference, ASCE, New York, Vol. 3: 1858-1870.

Fagherazzi, S., Bryan, K., Nardin, W., 2017. Buried Alive or Washed Away: The Challenging Life of Mangroves in the Mekong Delta. Oceanog. 30, 48–59. https://doi.org/10.5670/oceanog.2017.313

Folkard, A.M., 2019. Biophysical Interactions in Fragmented Marine Canopies: Fundamental Processes, Consequences, and Upscaling. Front. Mar. Sci. 6, 279. https://doi.org/10.3389/fmars.2019.00279

Fromard, F., Puig, H., Mougin, E., Marty, G., Betoulle, J.L., Cadamuro, L., 1998. Structure, above-ground biomass and dynamics of mangrove ecosystems: new data from French Guiana. Oecologia 115, 39–53. https://doi.org/10.1007/s004420050489

Ganthy, F., Soissons, L., Sauriau, P.-G., Verney, R., Sottolichio, A., 2015. Effects of short flexible seagrass Zostera noltei on flow, erosion and deposition processes determined using flume experiments. Sedimentology 62, 997–1023. https://doi.org/10.1111/sed.12170

Garzon, J.L., Maza, M., Ferreira, C.M., Lara, J.L., Losada, I.J., 2019. Wave Attenuation by Spartina Saltmarshes in the Chesapeake Bay Under Storm Surge Conditions. J. Geophys. Res. Oceans 124, 5220–5243. https://doi.org/10.1029/2018JC014865

Gourgue, O., Belzen, J., Schwarz, C., Bouma, T.J., Koppel, J., Temmerman, S., 2021. A Convolution Method to Assess Subgrid-Scale Interactions Between Flow and Patchy Vegetation in Biogeomorphic Models. J Adv Model Earth Syst 13. https://doi.org/10.1029/2020MS002116

Himes-Cornell, A., Grose, S.O., Pendleton, L., 2018. Mangrove Ecosystem Service Values and Methodological Approaches to Valuation: Where Do We Stand? Front. Mar. Sci. 5, 376. https://doi.org/10.3389/fmars.2018.00376

Hu, Z., Suzuki, T., Zitman, T., Uittewaal, W., Stive, M., 2014. Laboratory study on wave dissipation by vegetation in combined current–wave flow. Coastal Engineering 88, 131–142. https://doi.org/10.1016/j.coastaleng.2014.02.009

Jones, C.G., Lawton, J.H., Shachak, M., 1994. Organisms as Ecosystem Engineers. Oikos 69, 373. https://doi.org/10.2307/3545850

King, A.T., Tinoco, R.O., Cowen, E.A., 2012. A kε turbulence model based on the scales of vertical shear and stem wakes valid for emergent and submerged vegetated flows. J. Fluid Mech. 701, 1–39. https://doi.org/10.1017/jfm.2012.113

Liu, Z., Fagherazzi, S., She, X., Ma, X., Xie, C., Cui, B., 2020. Efficient tidal channel networks alleviate the drought-induced die-off of salt marshes: Implications for coastal restoration and management. Science of The Total Environment 749, 141493. https://doi.org/10.1016/j.scitotenv.2020.141493

Luhar, M., Nepf, H.M., 2011. Flow-induced reconfiguration of buoyant and flexible aquatic vegetation. Limnol. Oceanogr. 56, 2003–2017. ttps://doi.org/10.4319/lo.2011.56.6.2003

Maza, M., Adler, K., Ramos, D., Garcia, A.M., Nepf, H., 2017. Velocity and Drag Evolution From the Leading Edge of a Model Mangrove Forest: Velocity and Drag in a Mangrove

Forest. J. Geophys. Res. Oceans 122, 9144–9159. https://doi.org/10.1002/2017JC012945

Maza, M., Lara, J.L., Losada, I.J., 2019. Experimental analysis of wave attenuation and drag forces in a realistic fringe Rhizophora mangrove forest. Advances in Water Resources 131, 103376. https://doi.org/10.1016/j.advwatres.2019.07.006

Maza, M., Lara, J.L., Losada, I.J., Ondiviela, B., Trinogga, J., Bouma, T.J., 2015. Large-scale 3-D experiments of wave and current interaction with real vegetation. Part 2: Experimental analysis. Coastal Engineering 106, 73–86. https://doi.org/10.1016/j.coastaleng.2015.09.010

Mazda, Y., Magi, M., Motohiko, K., Hong, P.N., 1997. Mangroves as a coastal protection from waves in the Tong King delta, Vietnam. Mangroves Salt Marshes 1, 127–135. https://doi.org/10.1023/A:1009928003700

Mitsch, W.J., Gosselink, J.G., 2015. Wetlands, Fifth edition. ed. Wiley, Hoboken, New Jersey.

Morris, J.T., Sundareshwar, P.V., Nietch, C.T., Kjerfve, B., Cahoon, D.R., 2002. Responses of Coastal Wetlands to Rising Sea Level. Ecology 83, 2869–2877. https://doi.org/10.1890/0012-9658(2002)083[2869:ROCWTR]2.0.CO;2

Narayan, S., Beck, M.W., Reguero, B.G., Losada, I.J., van Wesenbeeck, B., Pontee, N., Sanchirico, J.N., Ingram, J.C., Lange, G.-M., Burks-Copes, K.A., 2016. The Effectiveness, Costs and Coastal Protection Benefits of Natural and Nature-Based Defences. PLoS ONE 11, e0154735. https://doi.org/10.1371/journal.pone.0154735

Nepf, H.M., Vivoni, E.R., 2000. Flow structure in depth-limited, vegetated flow. J. Geophys. Res. 105, 28547–28557. https://doi.org/10.1029/2000JC900145

Norris, B., 2019. Small-scale Turbulence and its Influence on Forest-scale Morphodynamics within a Coastal Mangrove Forest. The University of Waikato, Hamilton, New Zealand.

Norris, B.K., Mullarney, J.C., Bryan, K.R., Henderson, S.M., 2021. Relating millimeter-scale turbulence to meter-scale subtidal erosion and accretion across the fringe of a coastal mangrove forest. Earth Surf. Process. Landforms. 2021; 46: 573– 592. https://doi.org/10.1002/esp.5047

Paul, M., Bouma, T., Amos, C., 2012. Wave attenuation by submerged vegetation: combining the effect of organism traits and tidal current. Mar. Ecol. Prog. Ser. 444, 31–41. https://doi.org/10.3354/meps09489

Pinsky, M.L., Guannel, G., Arkema, K.K., 2013. Quantifying wave attenuation to inform coastal habitat conservation. Ecosphere 4, art95. https://doi.org/10.1890/ES13-00080.1

Quang Bao, T., 2011. Effect of mangrove forest structures on wave attenuation in coastal Vietnam. Oceanologia 53, 807–818. https://doi.org/10.5697/oc.53-3.807

San Juan, J. E., Veliz Carrillo, G., and Tinoco, R. O., 2019. Experimental observations of 3D flow alterations by vegetation under oscillatory flows. Environ Fluid Mech 19, 1497–1525. doi: 10.1007/s10652-019-09672-2

Schanderl, W., Jenssen, U., Manhart, M., 2017a. Near-Wall Stress Balance in Front of a Wall-Mounted Cylinder. Flow Turbulence Combust 99, 665–684. https://doi.org/10.1007/s10494-017-9865-3

Schanderl, W., Jenssen, U., Strobl, C., Manhart, M., 2017b. The structure and budget of turbulent kinetic energy in front of a wall-mounted cylinder. J. Fluid Mech. 827, 285–321. https://doi.org/10.1017/jfm.2017.486

Schoneboom, T., and Aberle, J., 2009. “Influence of foliage on drag force of flexible vegetation,” in Proceedings of IAHR.

Sharpe, R., James, C., 2007. Deposition of sediment from suspension in emergent vegetation. WSA 32, 211–218. https://doi.org/10.4314/wsa.v32i2.5244

Shepard, C.C., Crain, C.M., Beck, M.W., 2011. The Protective Role of Coastal Marshes: A Systematic Review and Meta-analysis. PLoS ONE 6, e27374. https://doi.org/10.1371/journal.pone.0027374

Suzuki, T., Zijlema, M., Burger, B., Meijer, M.C., Narayan, S., 2012. Wave dissipation by vegetation with layer schematization in SWAN. Coastal Engineering 59, 64–71. https://doi.org/10.1016/j.coastaleng.2011.07.006

Tanino, Y., Nepf, H.M., 2008. Lateral dispersion in random cylinder arrays at high Reynolds number. J. Fluid Mech. 600, 339–371. https://doi.org/10.1017/S0022112008000505

Temmerman, S., Bouma, T.J., Van de Koppel, J., Van der Wal, D., De Vries, M.B., Herman, P.M.J., 2007. Vegetation causes channel erosion in a tidal landscape. Geol 35, 631. https://doi.org/10.1130/G23502A.1

Temmink, R.J.M., Christianen, M.J.A., Fivash, G.S., Angelini, C., Boström, C., Didderen, K., Engel, S.M., Esteban, N., Gaeckle, J.L., Gagnon, K., Govers, L.L., Infantes, E., van Katwijk, M.M., Kipson, S., Lamers, L.P.M., Lengkeek, W., Silliman, B.R., van Tussenbroek, B.I., Unsworth, R.K.F., Yaakub, S.M., Bouma, T.J., van der Heide, T., 2020. Mimicry of emergent traits amplifies coastal restoration success. Nat Commun 11, 3668. https://doi.org/10.1038/s41467-020-17438-4

Tinoco, R. O., Coco, G., 2018. Turbulence as the main driver of resuspension in oscillatory flow through vegetation. Journal of Geophysical Research: Earth Surface, 123, 891– 904. https://doi.org/10.1002/2017JF004504

Tinoco, R.O., Coco, G., 2016. A laboratory study on sediment resuspension within arrays of rigid cylinders. Advances in Water Resources 92, 1–9. https://doi.org/10.1016/j.advwatres.2016.04.003

Tinoco, R. O., San Juan, J. E., and Mullarney, J. C., 2020. Simplification bias: lessons from laboratory and field experiments on flow through aquatic vegetation. Earth Surf. Process. Landforms 45, 121–143. doi: 10.1002/esp.4743

Vuik, V., Jonkman, S.N., Borsje, B.W., Suzuki, T., 2016. Nature-based flood protection: The efficiency of vegetated foreshores for reducing wave loads on coastal dikes. Coastal Engineering 116, 42–56. https://doi.org/10.1016/j.coastaleng.2016.06.001

Wang, C., Temmerman, S., 2013. Does biogeomorphic feedback lead to abrupt shifts between alternative landscape states? An empirical study on intertidal flats and marshes: SHIFTS BETWEEN INTERTIDAL FLAT AND MARSH. J. Geophys. Res. Earth Surf. 118, 229–240. https://doi.org/10.1029/2012JF002474

Widdows, J., Pope, N., Brinsley, M., 2008. Effect of Spartina anglica stems on near-bed hydrodynamics, sediment erodability and morphological changes on an intertidal mudflat. Mar. Ecol. Prog. Ser. 362, 45–57. https://doi.org/10.3354/meps07448

Whittaker, P., Wilson, C. A., and Aberle, J.,2015. An improved Cauchy number approach for predicting the drag and reconfiguration of flexible vegetation. Advances in Water Resources 83, 28–35. doi: 10.1016/j.advwatres.2015.05.005

Xie, D., Schwarz, C., Brückner, M.Z.M., Kleinhans, M.G., Urrego, D.H., Zhou, Z., van Maanen, B., 2020. Mangrove diversity loss under sea-level rise triggered by bio-morphodynamic feedbacks and anthropogenic pressures. Environ. Res. Lett. 15, 114033. https://doi.org/10.1088/1748-9326/abc122

Yagci, O., Celik, M.F., Kitsikoudis, V., Ozgur Kirca, V.S., Hodoglu, C., Valyrakis, M., Duran, Z., Kaya, S., 2016. Scour patterns around isolated vegetation elements. Advances in Water Resources 97, 251–265. https://doi.org/10.1016/j.advwatres.2016.10.002

Yang, J.Q., Nepf, H.M., 2018. A Turbulence-Based Bed-Load Transport Model for Bare and Vegetated Channels. Geophys. Res. Lett. 45. https://doi.org/10.1029/2018GL079319

Zhang, X., Chua, V.P., Cheong, H.-F., 2015. Hydrodynamics in mangrove prop roots and their physical properties. Journal of Hydro-environment Research 9, 281–294. https://doi.org/10.1016/j.jher.2014.07.010

Zhu, Z., Yang, Z., Bouma T.J. (2020) Biomechanical properties of marsh vegetation in space and time: effects of salinity, inundation and seasonality. Annals of Botany 125: 277–289, doi: 10.1093/aob/mcz063

Zong, L., Nepf, H., 2011. Spatial distribution of deposition within a patch of vegetation: Deposition pattern within a patch. Water Resour. Res. 47. https://doi.org/10.1029/2010WR009516